
Generating functional and multistate proteins with a multimodal diffusion transformer

Bowen Jing^{1†}, Anna Sappington^{1†}, Mihir Bafna¹, Ravi Shah², Adriana Tang¹,
Rohith Krishna³, Adam Klivans², Daniel J. Diaz², Bonnie Berger¹

¹MIT ²UT Austin ³University of Washington [†]Equal contribution

Abstract

Generating proteins with the full diversity and complexity of functions found in nature is a grand challenge in protein design. Here, we present ProDiT, a multimodal diffusion model that unifies sequence and structure modeling paradigms to enable the design of functional proteins at scale. Trained on sequences, 3D structures, and annotations for 214M proteins across the evolutionary landscape, ProDiT generates diverse, novel proteins that preserve known active and binding site motifs and can be successfully conditioned on a wide range of molecular functions, spanning 465 Gene Ontology terms. We introduce a diffusion sampling protocol to design proteins with multiple functional states, and demonstrate this protocol by scaffolding enzymatic active sites from carbonic anhydrase and lysozyme to be allosterically deactivated by a calcium effector. Our results showcase ProDiT’s unique capacity to satisfy design specifications inaccessible to existing generative models, thereby expanding the protein design toolkit.

1 Introduction

Generative models trained on datasets of protein sequences or backbone structures have enabled significant advances in *de novo* protein design [8, 44]. However, existing paradigms focus only on structure or sequence in isolation and are therefore fundamentally incapable of capturing the complete functional landscape of natural proteins. Structure generative models [42, 18, 22, 2] require hand-crafted specification of function in terms of a binding partner or functional motif [42] and are limited to the relatively scarce structural training data in the PDB. On the other hand, sequence generative models [25, 30, 14] cannot natively reason about sequence-structure-function relationships and have shown lower generation quality compared to structure generative models [4]. Neither family of approaches can target protein *dynamics*, a key feature of natural proteins, which often adopt multiple states to modulate their functions.

Here, we present ProDiT (Protein Diffusion Transformer), a novel framework that unifies structural and sequence generative modeling into a multimodal diffusion generative process, to enable these design capabilities. ProDiT leverages direct diffusion-based modeling of 3D structural coordinates alongside amino acid tokens using a fast, scalable transformer architecture. Our model design allows scaling multimodal training across large protein datasets, expanding beyond the PDB to the 214M available structures in AlphaFoldDB [37] and utilizing the full set of functional annotations in UniProtKB. In contrast to previous attempts at multimodal protein generative modeling such as ProteinGenerator [24] and ESM3 [14], our model matches or often exceeds the unconditional structure generation quality of RFDiffusion across all sequence lengths, while also significantly exceeding the sequence generation quality of dedicated protein language models (PLMs) like EvoDiff [4].

We explore ProDiT’s broad understanding of the protein sequence and structural landscape by conditioning generation on functional descriptors in the form of molecular function Gene Ontology (GO) terms. We conduct comprehensive benchmarking of ProDiT across 915 diverse GO terms

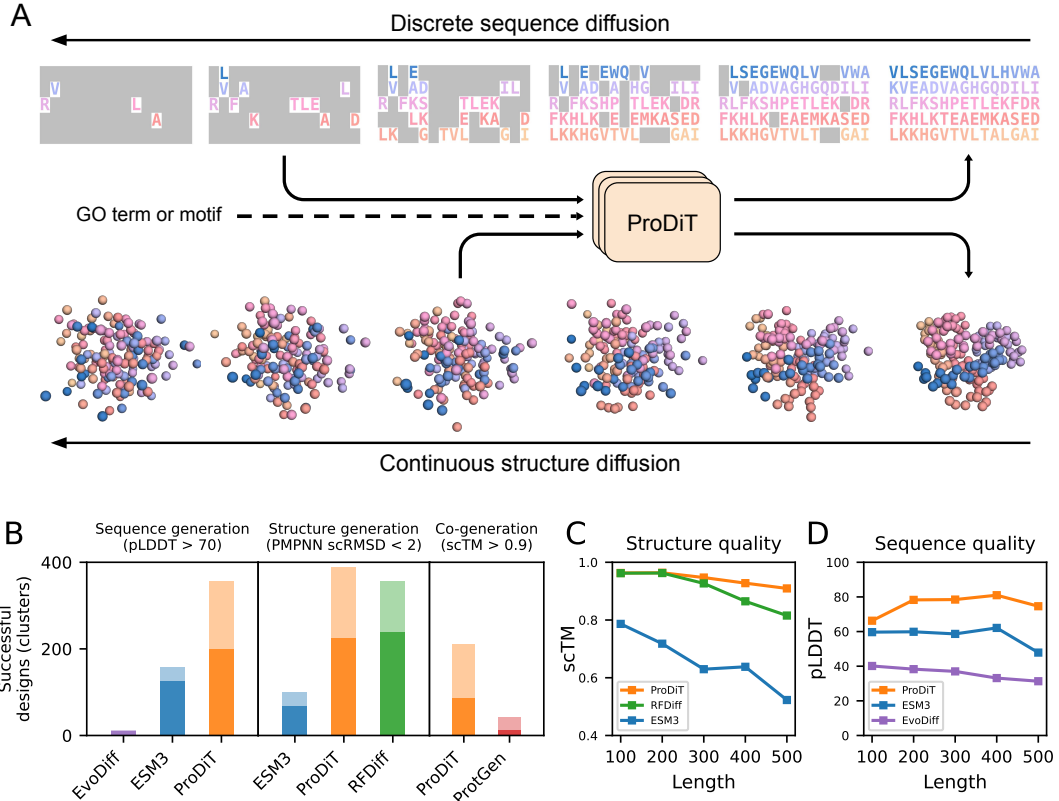


Figure 1: Overview of ProDiT and unconditional generation. **(A)** ProDiT is trained to denoise a joint diffusion process over sequence and structure. The two inputs may be at different noise levels, allowing for flexible generation workflows. **(B)** Comparison of ProDiT with other models by number of successful generations (light color) and unique FoldSeek clusters (dark color) from 500 samples (100 each of length 100, 200, 300, 400, 500). **(C)** Structure generation quality across protein lengths, measured in terms of self-consistency TM-score (scTM) between the generated structure and ProteinMPNN-designed sequence. **(D)** Sequence generation quality across protein lengths, measured in terms of ESMFold predicted Local Distance Difference Test (pLDDT).

representing highly specific descriptions of protein function and find generations predicted as functional for 463 of these terms, including terms represented in less than 0.01% of training examples in UniProtKB. Many of these generations have only moderate structural similarity to known functional proteins (TM-score < 0.7), showing an ability to generalize across the structural landscape. Structural alignments of our generations against known functional proteins reveal atomic-level recovery of active site residues, despite low global sequence similarity. We also develop a principled protocol for the design of dynamic, multistate proteins, derived from a novel interpretation of the sequence-structure-function paradigm based on probabilistic graphical models. We demonstrate our approach by scaffolding active sites from carbonic anhydrase and lysozyme to be allosterically modulated by calcium binding, an important step towards the design of custom and controllable enzymes.

2 Results

Multimodal Generation of Sequence and Structure ProDiT iteratively reverses two diffusion processes: one consisting of Gaussian noise added to the $\text{C}\alpha$ coordinates of centered protein structures and the other consisting of random masking of the amino acid sequence (Fig. 1A; **Methods**). At training time, the noise levels for sequence and structure are sampled independently; as a result, the model is able to denoise these modalities asynchronously, allowing for multiple generation workflows: sequence generation, structure generation (optionally followed by inverse folding), or sequence and structure co-generation. Additionally, ProDiT can accept as input structural or func-

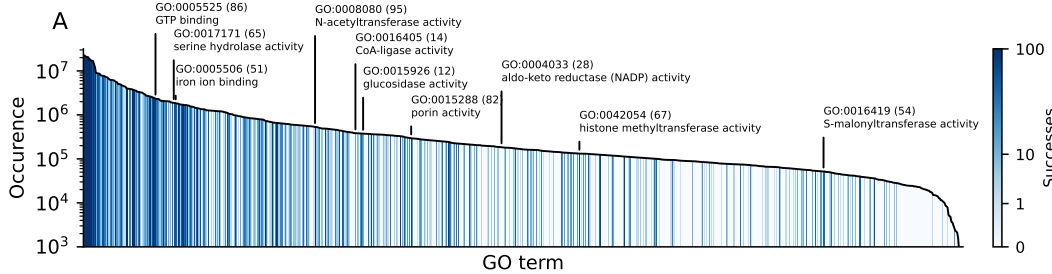


Figure 2: *In silico validation of molecular function conditioning.* For each of 915 molecular function GO terms sorted by occurrence in UniProtKB, we count the number of successful generations (out of 100), where success is defined as DeepFRI probability > 50% for the target term. Selected terms are labeled with the number of successes.

tional constraints in the form of motifs or molecular function Gene Ontology (GO) terms, respectively, for conditional generation. The model is trained and sampled with current best practices from the discrete and continuous diffusion literature (**Methods**).

We assess the performance of ProDiT in unconditional generation of sequence and structure according to standard metrics (Fig. 1B–D). For each method and modality, we draw 100 samples each of lengths 100, 200, 300, 400, and 500 amino acids and compute the total number of successful generations. ProDiT generates significantly more successful sequences than ESM3 and EvoDiff across all sequence lengths, surpasses the structure generation success rate of ESM3 [14], and matches the performance of RFDiffusion, a well-known structure generative model [42]. We observe similar trends when computing generation quality in terms of mean pLDDT or self-consistency TM-score (scTM) for sequence and structure, respectively (Fig. S1,S2). For co-generation, ProDiT produces self-consistent sequence and structure pairs when simultaneously denoising over both modalities (Fig. 1B, right), using a success cutoff of scTM > 0.9 after refolding with ESMFold. In contrast, ProteinGenerator is largely unable to generate self-consistent designs at lengths > 200 amino acids. Samples from the model in all three generation modalities are shown in Fig. 5E.

Steering Design with Molecular Function We assessed the responsiveness of ProDiT to functional conditioning with molecular function Gene Ontology (GO) terms with the DeepFRI function prediction network [12]. Each of 915 unique terms is associated with a median of 0.08% of proteins in UniProtKB (0.03%–0.26% IQR), providing a highly specific description of protein function. For each term, we generate 100 samples of length 300 amino acids from ProDiT (first generating the structure, then the sequence) and re-fold the sequence with ESMFold (**Methods**). A generation is counted as successful if the corresponding GO term is assigned by DeepFRI [12] with > 50% confidence for the refolded structure. In aggregate, 463 GO terms have at least one successful ProDiT design, with success rates being higher for the most prevalent GO terms and lower for less prevalent ones (Fig. 2A, 6B). As an orthogonal check of generation quality, we analyze the atomic fidelity of GO-conditioned generations in App. B.1. We assess the diversity of the generations by computing the TM-scores between successful designs with the same GO term and novelty via the TM-score to the most similar structure in AlphaFoldDB with the same GO term (Fig. 6C). We observe slightly improved diversity for more common GO terms versus less common terms (0.60 vs 0.66 TM-score, respectively), suggesting more robust generalization for frequently observed terms, although the novelty is similar (0.81 vs 0.78 TM-score, respectively).

Prior work in function-conditioned protein generation has often cited high structural similarity and low sequence identity to known functional proteins as a sign of generalization [25, 30]; however, this does not assess generalization across structures. Although the median successful ProDiT generation also has a high TM-score with known functional proteins, identifying the *most novel* design for each GO term reveals an average TM-score of 0.64 (across 169 assessed terms) to the closest neighbor in AlphaFoldDB with the same term, preserving the overall fold class but with significant local structural changes (Tab. S1). We identify and visualize these proteins for several terms in Fig. 6E.

Design of Multistate Allostery A significant challenge in protein design is the specification of complex, multistate functions, including allosteric regulation of protein activity [43, 24, 29, 13]. We

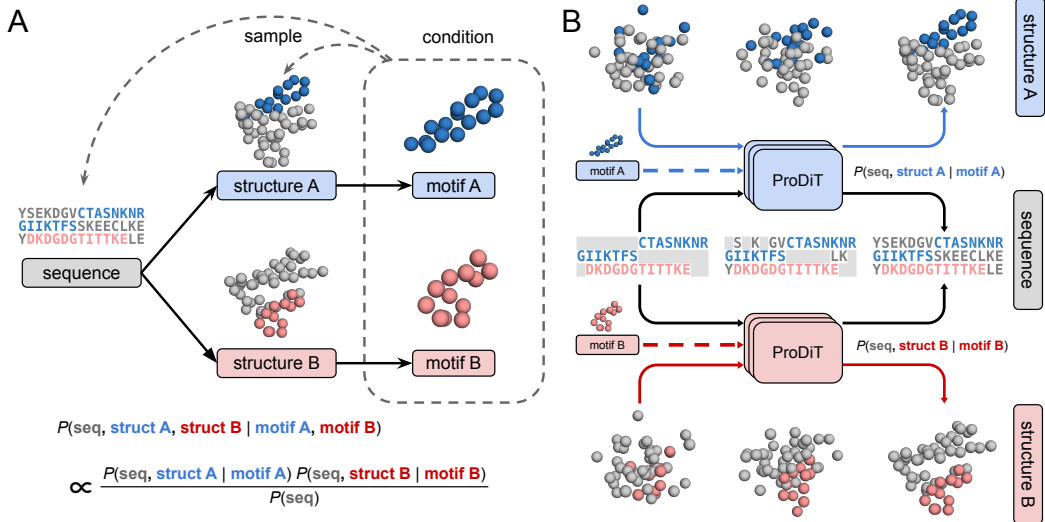


Figure 3: Coupled structure diffusion framework for generating multistate proteins. (A) The sequence-structure-function paradigm can be viewed as a directed graphical model in which structures are drawn from conditional densities $P(\text{struct} | \text{seq})$ and functions (here represented as motifs) are similarly drawn from structure. Multistate proteins correspond to sampling multiple conformers from the same sequence. Hence, designing a multistate protein amounts to conditioning on the two terminal variables (motifs) and sampling the parent variables (one sequence and two structures). This conditional probability can be written as the product of conditional probabilities that only involve at most a single structure. (B) The product density is heuristically sampled by coupling two structure and one sequence denoising trajectories, with two evaluations of the denoising model conditioned on the two different motifs. These evaluations correspond to the two product terms in the conditional probability. A third model evaluation corresponding to $P(\text{seq})$ is not shown.

hypothesized that a natively multimodal method that jointly samples sequence and structure could be well-suited for the direct generation of multistate proteins—protein sequences that can adopt multiple stable conformations. We formulate *coupled structure diffusion*, a principled technique for multistate design that requires models trained only on single state sequence-structure pairs. This technique, derived from a probabilistic graphical model interpretation of the sequence-structure-function paradigm (Figure 3A), involves two structure denoising trajectories that are constrained to a single sequence denoising trajectory. We iteratively denoise a structure with the active site motif (taken from PDB structures 1DPX and 6LUX, respectively) and a second structure with a 12-residue EF-hand calcium binding motif from calmodulin (1PRW) randomly inserted in the sequence. Both of these structure denoising trajectories share the same sequence trajectory. To evaluate whether we obtain an active and inactive conformation, we screened the designed sequences *in silico* by predicting the protein structure with Chai-1 [36] both with and without a calcium ion. When co-folding with calcium, a substantial fraction of generated structures shifted away (in terms of RMSD) from the active site motif and towards the EF-hand motif (Fig. 4A,B,I,J). We then identified sequence designs with low active site RMSD in the unbound state, low EF-hand RMSD in the bound state, and self-consistent Chai-1 predictions for both states. This subset allowed us to interpret and analyze the designed allosteric with greater confidence.

Scaffold for lysozyme (1DPX) active site motif

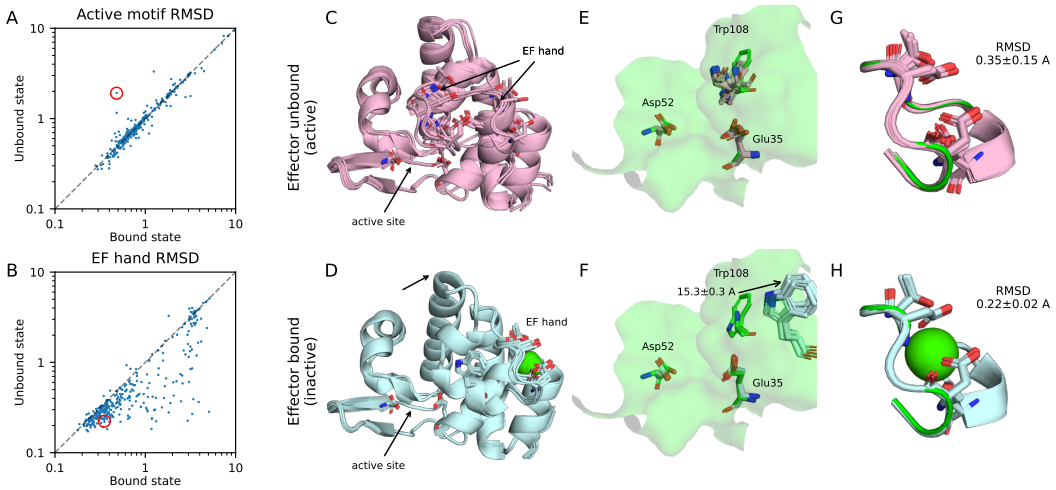


Figure 4: *In silico* validation of conformation switching designs. (A) For 320 designed scaffolds of the lysozyme motif, we refold the scaffold in both states with Chai-1 (inducing the bound state by co-folding with a calcium ion) and plot the resulting $C\alpha$ RMSDs for the four catalytic residues. The selected design is circled. (B) Corresponding $C\alpha$ RMSDs for the EF hand calcium binding motif. (C) Superimposed Chai-1 structure predictions (five total) of the unbound state. (D) Superimposed Chai-1 structure predictions (five total) of the bound state. (E,F) The surface mesh from the native enzyme is superimposed on the native and designed motifs, highlighting the catalytic residues Glu35 and Asp52. Note the large displacement of pocket-forming residue Trp108 (full motif shown in Fig. S11,S12). We report the mean and standard deviation of the displacement of the CH2 carbon. (G,H) The corresponding structures of the EF-hand calcium binding sites in the unbound and bound states, with the mean and standard deviation of the $C\alpha$ RMSD calculated.

In Fig. 4, we visualize the designed conformational change for the lysozyme motif (see App. B.2, Fig. 8 for carbonic anhydrase). The catalytic mechanism of lysozymes involves the formation of a covalent intermediate with Asp52 and uses Glu35 as a general acid to facilitate hydrolysis of a glycosidic bond [39]. This mechanism is representative of canonical glycosidase hydrolase chemistry, with the substrate specificity dictated by the surrounding microenvironment [39, 33]. For lysozymes, the Trp108 residue has been experimentally demonstrated to be critical for substrate recognition [19]. Furthermore, it is well established that carbohydrate C–H bonds interact preferentially with aromatic residues with tryptophan having a 9-fold enrichment in carbohydrate-binding modules (CBMs) [17]. In our selected design (Fig. 4A–H), Trp108 is scaffolded at its native position in the unbound state but is displaced by $\sim 15.3 \text{ \AA}$ in the calcium-bound state due to the rearrangement of several loops (Fig. 4E,F). This structural rearrangement indicates significant allosteric disruption of the substrate binding cleft, likely preventing the recognition and hydrolysis of the substrate.

3 Discussion

Here, we have presented ProDiT, a multimodal protein generative model that learns a function-aware joint distribution of sequence and structure. *In silico* metrics of unconditional generation quality indicate that ProDiT matches the performance of specialized, more expensive structural models and substantially outperforms multimodal approaches that discretize structure (ESM3 [14]) or map sequences to a continuous representation (ProteinGenerator [24]). Our comprehensive benchmarking of 915 GO terms provides, for the first time, predicted functional generations across a wide range of molecular functions, often demonstrating highly accurate recovery of known active site residues in structural alignments. Enabled by ProDiT’s multimodal capabilities, we have developed a novel protocol for multistate generation, marking an important step towards the design of custom and controllable enzymes. As researchers work to assemble a more complete picture of protein design with diverse biological functions, we anticipate ProDiT will serve as a blueprint for further developments in multimodal and multistate protein generative models.

Acknowledgments

We thank Samuel Sledzieski, Jeffrey O. Zhang, Amy Lu, Alexander Shida, Arvind Pillai, Jason Yim, Woody Ahern, and Soojung Yang for helpful discussions. This work was supported by the National Institute of General Medical Sciences of the National Institutes of Health under awards 1R35GM141861 (to B.B.) and T32GM144273 (via A.S.), the NSF AI Institute for Foundations of Machine Learning (IFML), the UT-Austin Center for Generative AI, and a gift from Param Hansa Philanthropies. B.J. was supported by a Department of Energy Computational Science Graduate Fellowship under Award Number DESC0022158. A.S. was supported by a Hertz Foundation Fellowship. R.K. was supported by the Advanced Research Projects Agency for Health APECx Program and a gift from Microsoft. This research used resources of the National Energy Research Scientific Computing Center (NERSC), a Department of Energy Office of Science User Facility using NERSC awards ASCR-ERCAP0027302, ASCR-ERCAP0030607, ASCR-ERCAP0032958, and ASCR-ERCAP0027818. The content is solely the responsibility of the authors and does not necessarily represent the official views of the National Institute of General Medical Sciences or the National Institutes of Health.

Competing Interests

D.J.D. owns Intelligent Proteins LLC where he consults biotechnology companies on AI protein engineering. D.J.D. is a co-founder of Metabolic AI, which focuses on developing commercial enzymes with AI. Other authors declare no competing interests.

References

- [1] Abramson, J., Adler, J., Dunger, J., Evans, R., Green, T., Pritzel, A., Ronneberger, O., Willmore, L., Ballard, A. J., Bambrick, J., et al. Accurate structure prediction of biomolecular interactions with alphafold 3. *Nature*, 630(8016):493–500, 2024.
- [2] Ahern, W., Yim, J., Tischer, D., Salike, S., Woodbury, S. M., Kim, D., Kalvet, I., Kipnis, Y., Coventry, B., Altae-Tran, H. R., et al. Atom level enzyme active site scaffolding using rfdiffusion2. *bioRxiv*, pp. 2025–04, 2025.
- [3] Ahmed Laskar, A. and Younus, H. Aldehyde toxicity and metabolism: the role of aldehyde dehydrogenases in detoxification, drug resistance and carcinogenesis. *Drug metabolism reviews*, 51(1):42–64, 2019.
- [4] Alamdari, S., Thakkar, N., van den Berg, R., Tenenholz, N., Strome, B., Moses, A., Lu, A. X., Fusi, N., Amini, A. P., and Yang, K. K. Protein generation with evolutionary diffusion: sequence is all you need. *BioRxiv*, pp. 2023–09, 2023.
- [5] Austin, J., Johnson, D. D., Ho, J., Tarlow, D., and Van Den Berg, R. Structured denoising diffusion models in discrete state-spaces. *Advances in neural information processing systems*, 34:17981–17993, 2021.
- [6] Barrio-Hernandez, I., Yeo, J., Jänes, J., Mirdita, M., Gilchrist, C. L., Wein, T., Varadi, M., Velankar, S., Beltrao, P., and Steinegger, M. Clustering predicted structures at the scale of the known protein universe. *Nature*, 622(7983):637–645, 2023.
- [7] Boone, C. D., Gill, S., Habibzadegan, A., and McKenna, R. Carbonic anhydrase: an efficient enzyme with possible global implications. *International Journal of Chemical Engineering*, 2013(1):813931, 2013.
- [8] Chu, A. E., Lu, T., and Huang, P.-S. Sparks of function by de novo protein design. *Nature biotechnology*, 42(2):203–215, 2024.
- [9] Dauparas, J., Anishchenko, I., Bennett, N., Bai, H., Ragotte, R. J., Milles, L. F., Wicky, B. I., Courbet, A., de Haas, R. J., Bethel, N., et al. Robust deep learning-based protein sequence design using proteinmpnn. *Science*, 378(6615):49–56, 2022.

- [10] Du, Y., Durkan, C., Strudel, R., Tenenbaum, J. B., Dieleman, S., Fergus, R., Sohl-Dickstein, J., Doucet, A., and Grathwohl, W. S. Reduce, reuse, recycle: Compositional generation with energy-based diffusion models and mcmc. In *International conference on machine learning*, pp. 8489–8510. PMLR, 2023.
- [11] Geffner, T., Didi, K., Zhang, Z., Reidenbach, D., Cao, Z., Yim, J., Geiger, M., Dallago, C., Kucukbenli, E., Vahdat, A., and Kreis, K. Proteina: Scaling flow-based protein structure generative models. In *The Thirteenth International Conference on Learning Representations*, 2025.
- [12] Gligorijević, V., Renfrew, P. D., Kosciolak, T., Leman, J. K., Berenberg, D., Vatanen, T., Chandler, C., Taylor, B. C., Fisk, I. M., Vlamakis, H., et al. Structure-based protein function prediction using graph convolutional networks. *Nature communications*, 12(1):3168, 2021.
- [13] Guo, A. B., Akpinaroglu, D., Stephens, C. A., Grabe, M., Smith, C. A., Kelly, M. J., and Kortemme, T. Deep learning-guided design of dynamic proteins. *Science*, 388(6749):eadr7094, 2025.
- [14] Hayes, T., Rao, R., Akin, H., Sofroniew, N. J., Oktay, D., Lin, Z., Verkuil, R., Tran, V. Q., Deaton, J., Wiggert, M., et al. Simulating 500 million years of evolution with a language model. *Science*, pp. eads0018, 2025.
- [15] Ho, J. and Salimans, T. Classifier-free diffusion guidance. *arXiv preprint arXiv:2207.12598*, 2022.
- [16] Ho, J., Jain, A., and Abbeel, P. Denoising diffusion probabilistic models. *Advances in neural information processing systems*, 33:6840–6851, 2020.
- [17] Hudson, K. L., Bartlett, G. J., Diehl, R. C., Aguirre, J., Gallagher, T., Kiessling, L. L., and Woolfson, D. N. Carbohydrate–aromatic interactions in proteins. *Journal of the American Chemical Society*, 137(48):15152–15160, 2015.
- [18] Ingraham, J. B., Baranov, M., Costello, Z., Barber, K. W., Wang, W., Ismail, A., Frappier, V., Lord, D. M., Ng-Thow-Hing, C., Van Vlack, E. R., et al. Illuminating protein space with a programmable generative model. *Nature*, 623(7989):1070–1078, 2023.
- [19] Inoue, M., Yamada, H., Yasukochi, T., Kuroki, R., Miki, T., Horiuchi, T., and Imoto, T. Multiple role of hydrophobicity of tryptophan-108 in chicken lysozyme: structural stability, saccharide binding ability, and abnormal pka of glutamic acid-35. *Biochemistry*, 31(24):5545–5553, 1992.
- [20] Johansson, K., Ramaswamy, S., Eklund, H., El-Ahmad, M., Hjelmqvist, L., and Jörnvall, H. Structure of betaine aldehyde dehydrogenase at 2.1 Å resolution. *Protein Science*, 7(10):2106–2117, 1998.
- [21] Karras, T., Aittala, M., Aila, T., and Laine, S. Elucidating the design space of diffusion-based generative models. *Advances in neural information processing systems*, 35:26565–26577, 2022.
- [22] Krishna, R., Wang, J., Ahern, W., Sturmels, P., Venkatesh, P., Kalvet, I., Lee, G. R., Morey-Burrows, F. S., Anishchenko, I., Humphreys, I. R., et al. Generalized biomolecular modeling and design with rosettafold all-atom. *Science*, 384(6693):eadl2528, 2024.
- [23] Lin, Y., Lee, M., Zhang, Z., and AlQuraishi, M. Out of many, one: Designing and scaffolding proteins at the scale of the structural universe with genie 2. *arXiv preprint arXiv:2405.15489*, 2024.
- [24] Lisanza, S. L., Gershon, J. M., Tipps, S. W., Sims, J. N., Arnoldt, L., Hendel, S. J., Simma, M. K., Liu, G., Yase, M., Wu, H., et al. Multistate and functional protein design using rosettafold sequence space diffusion. *Nature biotechnology*, pp. 1–11, 2024.
- [25] Madani, A., Krause, B., Greene, E. R., Subramanian, S., Mohr, B. P., Holton, J. M., Olmos Jr, J. L., Xiong, C., Sun, Z. Z., Socher, R., et al. Large language models generate functional protein sequences across diverse families. *Nature biotechnology*, 41(8):1099–1106, 2023.

- [26] Oefner, C., Schulz, H., D'Arcy, A., and Dale, G. E. Mapping the active site of escherichia coli malonyl-coa–acyl carrier protein transacylase (fabd) by protein crystallography. *Biological Crystallography*, 62(6):613–618, 2006.
- [27] Peebles, W. and Xie, S. Scalable diffusion models with transformers. In *Proceedings of the IEEE/CVF international conference on computer vision*, pp. 4195–4205, 2023.
- [28] Peng, F. Z., Bezemek, Z., Patel, S., Rector-Brooks, J., Yao, S., Tong, A., and Chatterjee, P. Path planning for masked diffusion model sampling. *arXiv preprint arXiv:2502.03540*, 2025.
- [29] Pillai, A., Idris, A., Philomin, A., Weidle, C., Skotheim, R., Leung, P. J., Broerman, A., Demakis, C., Borst, A. J., Praetorius, F., et al. De novo design of allosterically switchable protein assemblies. *Nature*, 632(8026):911–920, 2024.
- [30] Ruffolo, J. A., Nayfach, S., Gallagher, J., Bhatnagar, A., Beazer, J., Hussain, R., Russ, J., Yip, J., Hill, E., Pacesa, M., et al. Design of highly functional genome editors by modeling the universe of crispr-cas sequences. *BioRxiv*, pp. 2024–04, 2024.
- [31] Sahoo, S., Arriola, M., Schiff, Y., Gokaslan, A., Marroquin, E., Chiu, J., Rush, A., and Kuleshov, V. Simple and effective masked diffusion language models. *Advances in Neural Information Processing Systems*, 37:130136–130184, 2024.
- [32] Schiff, Y., Sahoo, S. S., Phung, H., Wang, G., Boshar, S., Dalla-torre, H., de Almeida, B. P., Rush, A. M., PIERROT, T., and Kuleshov, V. Simple guidance mechanisms for discrete diffusion models. In *The Thirteenth International Conference on Learning Representations*, 2025.
- [33] Shanmugam, N. S. and Yin, Y. Cazyme3d: a database of 3d structures for carbohydrate-active enzymes. *Journal of Molecular Biology*, pp. 169001, 2025.
- [34] Song, Y., Sohl-Dickstein, J., Kingma, D. P., Kumar, A., Ermon, S., and Poole, B. Score-based generative modeling through stochastic differential equations. In *International Conference on Learning Representations*, 2021.
- [35] Stams, T., Nair, S. K., Okuyama, T., Waheed, A., Sly, W. S., and Christianson, D. W. Crystal structure of the secretory form of membrane-associated human carbonic anhydrase iv at 2.8-å resolution. *Proceedings of the National Academy of Sciences*, 93(24):13589–13594, 1996.
- [36] team, C. D., Boitreaud, J., Dent, J., McPartlon, M., Meier, J., Reis, V., Rogozhonikov, A., and Wu, K. Chai-1: Decoding the molecular interactions of life. *BioRxiv*, pp. 2024–10, 2024.
- [37] Varadi, M., Bertoni, D., Magana, P., Paramval, U., Pidruchna, I., Radhakrishnan, M., Tsenvkov, M., Nair, S., Mirdita, M., Yeo, J., et al. AlphaFold protein structure database in 2024: providing structure coverage for over 214 million protein sequences. *Nucleic acids research*, 52(D1):D368–D375, 2024.
- [38] Vaswani, A., Shazeer, N., Parmar, N., Uszkoreit, J., Jones, L., Gomez, A. N., Kaiser, Ł., and Polosukhin, I. Attention is all you need. *Advances in neural information processing systems*, 30, 2017.
- [39] Vocadlo, D. J., Davies, G. J., Laine, R., and Withers, S. G. Catalysis by hen egg-white lysozyme proceeds via a covalent intermediate. *Nature*, 412(6849):835–838, 2001.
- [40] Wang, J., Lisanza, S., Juergens, D., Tischer, D., Watson, J. L., Castro, K. M., Ragotte, R., Saragovi, A., Milles, L. F., Baek, M., et al. Scaffolding protein functional sites using deep learning. *Science*, 377(6604):387–394, 2022.
- [41] Wang, X., Zheng, Z., Ye, F., Xue, D., Huang, S., and Gu, Q. Diffusion language models are versatile protein learners. In *International Conference on Machine Learning*, pp. 52309–52333. PMLR, 2024.
- [42] Watson, J. L., Juergens, D., Bennett, N. R., Trippe, B. L., Yim, J., Eisenach, H. E., Ahern, W., Borst, A. J., Ragotte, R. J., Milles, L. F., et al. De novo design of protein structure and function with rfdiffusion. *Nature*, 620(7976):1089–1100, 2023.

- [43] Wei, K. Y., Moschidi, D., Bick, M. J., Nerli, S., McShan, A. C., Carter, L. P., Huang, P.-S., Fletcher, D. A., Sgourakis, N. G., Boyken, S. E., et al. Computational design of closely related proteins that adopt two well-defined but structurally divergent folds. *Proceedings of the National Academy of Sciences*, 117(13):7208–7215, 2020.
- [44] Winnifrith, A., Outeiral, C., and Hie, B. Generative artificial intelligence for de novo protein design. *Current Opinion in Structural Biology*, 86:102794–102794, 2024.

A Methods

A.1 Multimodal Diffusion

ProDiT models protein sequence as strings in the discrete amino acid vocabulary $\mathbf{s} \in [1, 20]^L$ and C α protein structure as an element of Euclidean space $\mathbf{x} \in \mathbb{R}^{3L}$. The model learns to generate the data distribution by reversing noising processes defined directly on these spaces (i.e., without tokenization or embedding); as such, its training and inference formulations invoke both continuous and discrete diffusion, described below. Our training loss is a weighted combination of the structure and sequence losses, $\mathcal{L} = \mathcal{L}_{\text{struct}} + 3\mathcal{L}_{\text{seq}}$.

A.1.1 Continuous diffusion.

In diffusion modeling of continuous data $\mathbf{x} \in \mathbb{R}^d$, the data distribution p_{data} is corrupted under a forward diffusion process $d\mathbf{x} = f(\mathbf{x}, t) dt + g(t) d\mathbf{w}$ where \mathbf{w} is Brownian motion. This generates a time-evolving density $p_t(\mathbf{x}), t \in [0, T]$ with initial conditions $p_0 = p_{\text{data}}$ and p_T close to Gaussian. The diffusion process can be simulated in reverse via $d\mathbf{x} = [-f(\mathbf{x}, t) + g^2(t)\nabla \log p_t(\mathbf{x})] dt + g(t) d\bar{\mathbf{w}}$ with use of the so-called score $\nabla \log p_t(\mathbf{x})$ [16, 34]. We approximate $\nabla \log p_t(\mathbf{x})$ with a neural network $s_\theta(\mathbf{x})$ by minimizing the MSE denoising score matching objective $\mathbb{E}_{\mathbf{x}_0, \mathbf{x}_t} [| | s_\theta(\mathbf{x}, t) - \nabla_{\mathbf{x}_t} \log p_{t|0}(\mathbf{x}_t | \mathbf{x}_0) | |^2]$ for all t . To apply diffusion modeling to protein structure, we take $n = 3L$ and \mathbf{x} to be the zero-mean coordinates of the C α atoms. We adapt, with minor notational modifications, the parameterization of Karras et al [21]: $f(\mathbf{x}, t) = 0, g(t) = \sqrt{2t}$ such that $p_{t|0}(\mathbf{x}_t | \mathbf{x}_0) = \mathcal{N}(\mathbf{x}_t; \mu = \mathbf{x}_0, \Sigma = t^2 \mathbf{I}_n)$. We then define time rescaling

$$t' = \frac{t^{1/p} - t_{\min}^{1/p}}{t_{\max}^{1/p} - t_{\min}^{1/p}} \quad (1)$$

with $t_{\min} = 0.05 \text{ \AA}$, $t_{\max} = 160 \text{ \AA}$, $p = 7$ and train for times $t' \in [0, 1]$. That is, the neural network is trained to remove Gaussian noise ranging from $\sigma = 0.05 \text{ \AA}$ to $\sigma = 160 \text{ \AA}$. The neural network score model is parameterized with post-conditioning, i.e.,

$$\mathbf{s}_\theta(\mathbf{x}, t) = \frac{1}{t^2} \left[\frac{t \cdot t_{\text{data}}}{\sqrt{t_{\text{data}}^2 + t^2}} f_\theta(\mathbf{x}, t) - \frac{t^2}{t_{\text{data}}^2 + t^2} \mathbf{x} \right] \quad (2)$$

where $t_{\text{data}} = 15 \text{ \AA}$ and $f_\theta(\mathbf{x}, t)$ is the neural network. We observe that in the limit of $t \rightarrow 0$ we have $\mathbf{s}_\theta(\mathbf{x}, t) \approx f_\theta(\mathbf{x}, t)/t$ and in the limit of $t \rightarrow \infty$ we have $\mathbf{s}_\theta(\mathbf{x}, t) \approx (t_{\text{data}} f_\theta(\mathbf{x}, t) - \mathbf{x})/t^2$. Hence, the network interpolates between predicting the score and predicting the clean data.

Our final structure training loss is then

$$\mathcal{L}_{\text{struct}} = \mathbb{E}_{t' \sim U[0, 1], \mathbf{x}_0, \mathbf{x}_t} \left[\frac{t^2(t^2 + t_{\text{data}}^2)}{t_{\text{data}}^2} | | s_\theta(\mathbf{x}_t, t) - \nabla_{\mathbf{x}_t} \log p_{t|0}(\mathbf{x}_t | \mathbf{x}_0) | |^2 \right] \quad (3)$$

At inference time, we sample $\mathbf{x}_{t_{\max}} \sim \mathcal{N}(0, t_{\max}^2 \mathbf{I})$ and integrate from $t' = 1$ to $t' = 0$ with the Euler-Maruyama scheme with uniform steps in t' . We apply low temperature annealing and modify the reverse diffusion as

$$d\mathbf{x} = \left[\frac{g^2(t)}{2} (1 + \beta(t)) s_\theta(\mathbf{x}, t) \right] dt + g(t) \beta(t) \gamma(t) d\bar{\mathbf{w}} \quad (4)$$

where $\gamma(t) = 0.5$ and $\beta(t) = 1/(1 + t/t_{\text{data}})^\nu$. Here $\beta(t)$ controls the stochasticity via mixing level of Langevin dynamics and $\gamma(t)$ controls the temperature of the dynamics. We use $\nu = 0.5$ for unconditional generation and $\nu = 1$ for conditional generation. As in prior work, we find these low temperature dynamics essential for generating high quality structures [18, 11].

A.1.2 Discrete diffusion.

In diffusion modeling of discrete data [5], we represent an element of the vocabulary with its one-hot vector and transport the data distribution $p_0 = p_{\text{data}}$ towards a prior with probability vector $\boldsymbol{\pi} \in \Delta^K$, where Δ^K is the K -simplex. In particular, we define a corruption schedule $\alpha_t, t \in [0, 1]$ such that $\alpha_0 = 1, \alpha_1 = 0$ monotonically decreasing and a noising process

$p_{t|s}(\mathbf{x}_t \mid \mathbf{x}_s) = \text{Cat}(\mathbf{x}_t; (\alpha_t/\alpha_s)\mathbf{x}_s + (1 - \alpha_t/\alpha_s)\boldsymbol{\pi})$ for $t > s$. This generates noisy marginals $p_t(\mathbf{x}_t) = \sum_{\mathbf{x}_0} \text{Cat}(\mathbf{x}_t; \alpha_t \mathbf{x}_0 + (1 - \alpha_t)\boldsymbol{\pi}) p(\mathbf{x}_0)$. The noising process can be reversed by iteratively sampling

$$p_{s|t}(\mathbf{x}_s \mid \mathbf{x}_t) = \sum_{\mathbf{x}_0} p(\mathbf{x}_s \mid \mathbf{x}_t, \mathbf{x}_0) p(\mathbf{x}_0 \mid \mathbf{x}_t) \quad (5)$$

where $p(\mathbf{x}_s \mid \mathbf{x}_t, \mathbf{x}_0)$ is analytically computed from Bayes' rule and we approximate $p(\mathbf{x}_0 \mid \mathbf{x}_t) \approx \text{Cat}(\mathbf{x}_0; \hat{\mathbf{x}}_0(\mathbf{x}_t; \theta))$ via a neural network $\hat{\mathbf{x}}_0(\mathbf{x}_t; \theta) \in \Delta^K$. The network is trained by minimizing the cross entropy $\mathbb{E}_{\mathbf{x}_0, \mathbf{x}_t} [-\log(\hat{\mathbf{x}}_0(\mathbf{x}_t; \theta), \mathbf{x}_0)]$ for all t . To apply discrete diffusion to protein sequences, we noise all positions independently and adopt the parameterization of MDLM [31] and DPLM [41]. In particular, we let $K = 21$ and define the K^{th} state to represent a mask state \mathbf{m} . We then assign $\boldsymbol{\pi} = \mathbf{m}$. With this parameterization, the reverse process becomes

$$p_{s|t}(\mathbf{x}_s \mid \mathbf{x}_t) = \text{Cat}\left(\mathbf{x}_s; (1 - \delta_{\mathbf{x}_t, \mathbf{m}})\mathbf{x}_t + \delta_{\mathbf{x}_t, \mathbf{m}} \left[\frac{1 - \alpha_s}{1 - \alpha_t} \mathbf{m} + \frac{\alpha_s - \alpha_t}{1 - \alpha_t} \hat{\mathbf{x}}_0(\mathbf{x}_t; \theta) \right] \right) \quad (6)$$

Note that the sampling is independent across positions but the neural network $\hat{\mathbf{x}}_0(\mathbf{x}_t; \theta)$ takes the entire sequence as input (for brevity we omit this distinction in notation).

Our final sequence training loss is then

$$\mathcal{L}_{\text{seq}} = \mathbb{E}_{t \sim U[0,1], \mathbf{x}_0, \mathbf{x}_t} [-\lambda(t) \delta_{\mathbf{x}_t, \mathbf{m}} \log \langle \hat{\mathbf{x}}_0(\mathbf{x}_t; \theta), \mathbf{x}_0 \rangle] \quad (7)$$

where $\lambda(t) = 1 - t$ as in DPLM. Notably, only the logits of positions where $\mathbf{x}_t = \mathbf{m}$ are supervised.

For inference, we initially set $\mathbf{x}_1 = \mathbf{m}$ and iteratively sample \mathbf{x}_t with steps uniform in t . The sampling strategy depends on the task. For unconditional sequence generation, our sampling deviates from ancestral sampling of the reverse process $p_{s|t}$ and instead follows the approach introduced in DPLM [41], which can be cast as self-planning under a Path Planning framework [28]. Specifically, a single step from t to s with $t > s$ and L being the sequence length proceeds as follows:

$$z_{\ell,i} \sim \text{Gumbel}(1, 1), \text{shape}(z) = [L, 20] \quad (8)$$

$$\phi_{\ell,i} \leftarrow \log \text{softmax}_i((\text{logits}(\hat{\mathbf{x}}_0(\mathbf{x}_t; \theta))_{\ell,i} + z_{\ell,i}) / \gamma(t)) \quad (9)$$

$$y_\ell, u_\ell \leftarrow \arg \max_i \phi_{\ell,i}, \max_i \phi_{\ell,i} \quad (10)$$

$$S_{\text{topk}} \leftarrow \text{topk}_\ell(u_\ell, k = L - \text{round}(sL)), S_{\text{topk}} \subseteq [1 \dots L] \quad (11)$$

$$(\mathbf{x}_s)_\ell = \begin{cases} y_\ell & \ell \in S_{\text{topk}} \wedge (\mathbf{x}_t)_\ell = \mathbf{m} \\ (\mathbf{x}_t)_\ell & \ell \in S_{\text{topk}} \wedge (\mathbf{x}_t)_\ell \neq \mathbf{m} \\ \mathbf{m} & \ell \notin S_{\text{topk}} \end{cases} \quad (12)$$

Here, $\gamma(t)$ is a temperature and we set $\gamma(t) = 0.5$ for sequence generation. In co-generation, we follow a similar procedure except $\gamma(t) = 0.1 + 0.4t$ and instead set

$$y_\ell, u_\ell \leftarrow (\mathbf{x}_t)_\ell, \phi_{\ell, (\mathbf{x}_t)_\ell} \quad (13)$$

for ℓ such that $(\mathbf{x}_t)_\ell \neq \mathbf{m}$; that is, the sampled token and log probability are replaced with the current token and its log probability under the model prediction. Finally, in inverse folding, we choose a random unmasking order and sample each position with temperature 0.1, as done in ProteinMPNN [9].

A.2 Model Architecture and Training

ProDiT is a transformer architecture [38] based closely on the design of diffusion transformers for images [27]. In particular, it consists of 30 transformer blocks, each with a self-attention block and feed-forward layer. We adopt adaLN-Zero [27] to inject conditioning information, in particular a sinusoidal embedding of the structural diffusion time. We follow modern transformer best practices, including pre-norm, QK-norm, and GeLU activations. Unconventionally, we adopt a dropout rate of 20%, which we found essential for sequence generation performance.

The model accepts four types of inputs: structure, sequence, motifs, and GO terms. The structure is directly embedded with a linear layer without any geometric or equivariant transformations, following emerging best practice [1, 11]. The sequence is embedded with a learned embedding. The

motifs are centered and also embedded with a linear layer, with motif positions additionally marked with a learned embedding in both the model input and adaLN-Zero conditioning. Finally, the GO terms are input via a learned embedding vector for each term. ProDiT then outputs via two linear heads a structural output for continuous structural diffusion and classifier logits for discrete sequence diffusion.

We train two models: one with model dimensionality 768 (without function conditioning) and one with model dimensionality 1024 (with function conditioning). These models have 321M and 576M parameters, respectively. Both models are trained with crop size 512 and batch size 250k–500k tokens across 16–32 NVIDIA H200 GPUs for approximately 500k steps. Model parameters are tracked with an exponential moving average with decay coefficient 0.999. 50% of the time, we sample motif conditioning following the motif sampling algorithm in Genie2 [23]. When GO terms are available, 85% of the time we sample a term at random in proportion to its inverse frequency across in UniProtKB, whereas 15% of the time we drop the GO term. Additionally, we completely drop the sequence or structure each 5% of the time.

A.3 Data

Our training set is drawn from 214M proteins in UniProtKB which have associated structures in AlphaFoldDB. Unlike prior work on protein language models, we cluster proteins for training by structural similarity rather than sequence similarity; we found this to improve generation diversity. Specifically, we use the FoldSeek clusterings of AlphaFoldDB computed by Barrio-Hernandez et al [6] as hierarchical clusters; we first sample a random FoldSeek cluster, then a random MMseqs cluster within the FoldSeek cluster, and finally a random protein within the MMseqs cluster. At training time, we filter to sample proteins with PLDDT > 80; this results in 1.24M FoldSeek clusters, 18.9M MMseqs clusters, and 128M sequences.

To obtain function training data, we compile metadata from all UniProtKB entries and associate each entry with the set of all molecular function GO terms listed in the entry and any implied parent molecular function terms not already present (via “is_a” relationship types listed in <http://purl.obolibrary.org/obo/go/go.obo>). 65% of entries contain at least one non-root term, with those entries having 9.6 terms on average. We then compute frequencies of each term in our training dataset order to sample them according to inverse frequency at training time. The resulting set of 8220 terms comprises the input vocabulary of ProDiT.

A.4 Design and Evaluation

We use the 321M-parameter model for unconditional generation protocols, as it obtains slightly better diversity, and use the 576M-parameter model for conditional generation.

A.4.1 Unconditional generation.

For sequence generation, we sample a noisy structure at the highest noise level and fix it while iteratively unmasking the sequence. For structure generation, we initialize and fix the sequence to be the all-mask state while denoising the structure. We then design 8 sequences using ProteinMPNN, refold each of them with ESMFold, and keep the sequence with the lowest self-consistency RMSD. For co-generation, we denoise both modalities with a linear schedule and report self-consistency metrics (scRMSD, scTM) using the sequence designed by ProDiT. In all modalities, we sample generations of length L using L model forward passes. To compute the number of successful clusters, we pool all successful generations from different lengths and run FoldSeek clustering via:

```
foldseek easy-cluster <dir> <out> <tmp> --alignment-type 1 --cov-mode 0  
--min-seq-id 0 --tm-score-threshold 0.5
```

We use the ESMFold structures for sequence generation and the raw ProDiT outputs for structure generation and co-generation.

To benchmark against prior work, we download the code and weights for ESM3 1.4B, RFDiffusion, EvoDiff 640M, ProteinGenerator from their public websites. For ESM3, because default sampling settings are not provided, we experimented with sampling hyperparameters and found the following settings to yield the best results: sequence is sampled with linear schedule, L steps, random order, and temperature 1; and structure is sampled with linear schedule, L steps, random order, and tem-

perature 0.8. For RFDiffusion and ProteinGenerator, we use the default sampling scripts but set the number of diffusion steps to be 50 for ProteinGenerator (default 25). We use the Genie2 evaluation pipeline [23] to run ProteinMPNN on generated structures and assess all structure generation methods.

A.4.2 Function conditioning.

The DeepFRI function prediction network outputs predictions for 942 distinct molecular function GO terms, 915 of these are in the input vocabulary of ProDiT (most of the excluded terms have been marked obsolete). For each of these terms, we generate 100 proteins of length 300 by first generating a structure in 300 steps, then a corresponding sequence (using inverse folding sampling) in 300 additional steps. All sequences are refolded with ESMFold. Because some GO terms may correspond to proteins with disordered regions or flexible interdomain orientations, we do not filter based on scTM or scRMSD. The generation is marked as successful if DeepFRI predicts a probability $\geq 50\%$ for the desired GO term from the refolded structure. We run DeepFRI with the command:

```
python predict.py --pdb_dir <dir> --ont mf --output_fn_prefix <out>
```

To compute the diversity, we gather all successful generations with the same GO term and compute the TM-score between generations i, j via TMalign. The diversity of generation i is then the mean of $TM_{i,j}, i \neq j$. Note that $TM_{i,j} = TM_{j,i}$ as all generations have the same length. We display histograms of diversity TM-scores of successful generations pooled across all terms (Fig. 2C), i.e., terms with more successes have higher weight.

To compute the novelty of the generations, we first compile a FoldSeek database for selected GO terms by gathering all AlphaFoldDB structures with the target GO term and running:

```
foldseek createdb <pdb_dir> <out_db>
```

We query this database via

```
foldseek easy-search <query_pdbs> <go_db> <out> <tmp> --alignment-type 1  
--format-output query,target,alntmscore,qtmscore
```

We then take the match with the highest qtmscore found by foldseek, i.e., the TM-score normalized by the length of the query (300) and assign this as the novelty TM-score of the generated protein. This ensures that high TM-scores correspond to a match for the entire generated protein rather than a short AlphaFoldDB protein matching part of the generated structure. Because of the relatively high runtime of this protocol, we only compute novelty results for 169 GO terms randomly selected from those with 10 or more success and 2M or fewer occurrences. We display histograms of novelty TM-scores of successful generations pooled across all terms (Fig. 2C), i.e., terms with more successes have higher weight.

To implement classifier-free guidance for function conditioning, we follow prior literature [15, 32] and run denoising sampling with linear combinations of logits (in discrete spaces) or scores (in continuous spaces). Let $\phi(\mathbf{s}, \mathbf{x}, t_{\text{seq}}, t_{\text{struct}} | \emptyset)$ and $\phi(\mathbf{s}, \mathbf{x}, t_{\text{seq}}, t_{\text{struct}} | c)$ represent the output of ProDiT when denoising sequence \mathbf{s} and structure \mathbf{x} unconditionally and conditioned on functional class c , respectively. Then for guidance strength λ , we denoise with

$$(1 - \lambda)\phi(\mathbf{s}, \mathbf{x}, t_{\text{seq}}, t_{\text{struct}} | \emptyset) + \lambda\phi(\mathbf{s}, \mathbf{x}, t_{\text{seq}}, t_{\text{struct}} | c) \quad (14)$$

A.4.3 Structural alignment pipeline.

To further verify that function-conditioned generations are biologically meaningful, we design a pipeline that compares the active sites of generated structures with experimental structures from AlphaFoldDB (AFDB) of the same GO term.

For each GO term, we filter UniProtKB for entries with AFDB structures and at least 2 labeled active site residues in the entry's UniProtKB feature table (sufficiently annotated). Each generated structure is then structurally aligned to all sufficiently annotated AFDB structures with the same GO term using `gemmi.calculate_superposition` with selection on protein backbone atoms via `gemmi.SupSelect.MainChain`. For each labeled active site residue in the AFDB structure's UniProtKB feature table, we identify the nearest residue in the generated structure with (i) the same amino acid type (ii) minimized Euclidean distance between any atom in the generated and AFDB

residues. If a one-to-one correspondence was found for all annotated active site residues, we computed the all atom RMSD of the active sites. To compute the RMSD, atom positions were directly paired based on name correspondence, and the final RMSD was reported as the root mean square of the interatomic distances across the full set of matched residue pairs. Alignments with this RMSD below 1.0 Å were considered successful confirmations of active site conservation. Due to long runtimes, this process was applied to 337 GO terms.

For each successful generated structure with confirmed active site matches, we further analyzed the structure by comparing them to their five closest AFDB structures (ranked by lowest active site RMSD). For each of these structure pairs, we computed several metrics, including the global backbone RMSD, the RMSD of the active site, and the RMSDs of expanded regions around the active site using spherical expansions from 1 Å to 18 Å. All RMSD values were computed in PyMOL after realigning the structures on the selected active site or expanded region. For each level of expansion, we also match the residues in the generated structure to the closest reference residue (post-alignment) and compute the fraction of matched residue identities.

A.4.4 Multistate design.

The objective of our multistate design protocol is to sample a single sequence \mathbf{x} which folds into two distinct structures, $\mathbf{x}_1, \mathbf{x}_2$, supporting functional motifs $\mathbf{m}_1, \mathbf{m}_2$, respectively. Using the conditional independencies implied by the directed graphical model, we can rewrite this target conditional distribution as:

$$p(\mathbf{s}, \mathbf{x}_1, \mathbf{x}_2 | \mathbf{m}_1, \mathbf{m}_2) \propto p(\mathbf{s}, \mathbf{x}_1, \mathbf{x}_2, \mathbf{m}_1, \mathbf{m}_2) \quad (15)$$

$$= p(\mathbf{s})p(\mathbf{x}_1 | \mathbf{s})p(\mathbf{x}_2 | \mathbf{s})p(\mathbf{m}_1 | \mathbf{s}, \mathbf{x}_1)p(\mathbf{m}_2 | \mathbf{s}, \mathbf{x}_2) \quad (16)$$

$$= p(\mathbf{s}) \frac{p(\mathbf{s}, \mathbf{x}_1)}{p(\mathbf{s})} \frac{p(\mathbf{s}, \mathbf{x}_2)}{p(\mathbf{s})} \frac{p(\mathbf{s}, \mathbf{x}_1 | \mathbf{m}_1)p(\mathbf{m}_1)}{p(\mathbf{s}, \mathbf{x}_1)} \frac{p(\mathbf{s}, \mathbf{x}_2 | \mathbf{m}_2)p(\mathbf{m}_1)}{p(\mathbf{s}, \mathbf{x}_2)} \quad (17)$$

$$\propto \frac{p(\mathbf{s}, \mathbf{x}_1, | \mathbf{m}_1)p(\mathbf{s}, \mathbf{x}_2, | \mathbf{m}_2)}{p(\mathbf{s})} \quad (18)$$

Each of these terms corresponds to our learned generative model under some form of conditioning: $p(\mathbf{s}, \mathbf{x}_i | \mathbf{m}_i)$ is the distribution sampled by motif scaffolding \mathbf{m}_i , and $p(\mathbf{s})$ is the distribution sampled by unconditional sequence generation. The product (and ratio) of these densities cannot be directly sampled by diffusion models; however, heuristic procedures for sampling similar densities involving the linear combinations of logits (in discrete spaces) and scores (in continuous spaces) are widely employed in the generative modeling literature [10], using the property that logarithms of products (and ratios) of densities are sums (and differences) of log densities.

Hence, we suggest a heuristic sampling algorithm for sampling the target density as follows: let $\phi(\mathbf{s}, \mathbf{x}_i, t_{\text{seq}}, t_{\text{struct}} | \mathbf{m}_i)$ and $\psi(\mathbf{s}, \mathbf{x}_i, t_{\text{seq}}, t_{\text{struct}}, | \mathbf{m}_i)$ represent the logits and score predictions, respectively, of neural networks provided noisy sequence \mathbf{s} , and noisy structure \mathbf{x}_i , diffusion times $t_{\text{seq}}, t_{\text{struct}}$, and motif \mathbf{m}_i . Then we denoise the sequence \mathbf{s} with logits

$$\phi(\mathbf{s}, \mathbf{x}_1, t_{\text{seq}}, t_{\text{struct}} | \mathbf{m}_1) + \phi(\mathbf{s}, \mathbf{x}_2, t_{\text{seq}}, t_{\text{struct}}, | \mathbf{m}_2) - \phi(\mathbf{s}, t_{\text{seq}}) \quad (19)$$

and denoise each noisy structure \mathbf{x}_i with scores $\psi(\mathbf{s}, \mathbf{x}_i, t_{\text{seq}}, t_{\text{struct}} | \mathbf{m}_i)$. We use these expressions as logits and scores of a black-box model output and proceed with the same discrete and continuous sampling algorithms as described previously.

To explore the application this pipeline to allosteric regulation of enzymes, we posit that a multistate enzyme could be designed via two explicit structural states: one to scaffold the desired active site motif, and another to scaffold the binding motif of a desired effector. (Although there is a risk that the model would produce a degenerate design of a single or very similar structures scaffolding both motifs, we find that this does not occur in a typical sample.) We select calcium as the effector and the EF hand motif in positions 20–31 in PDB 1PRW as the effector binding motif.

For the carbonic anhydrase active site motif, we select the all residues from PDB 6LUX with C α coordinate within 7 Å if the position of the zinc cofactor. For the lysozyme active site motif, we first compute the midpoint of a line connecting the C α atoms of catalytic residues Glu35 and Asp52 in PDB 1DPX, and include all residues with C α coordinate within 8 Å of this midpoint. We sample 320 designs for each active site motif, using 200 (carbonic anhydrase) or 500 (lysozyme) steps of sequence-structure co-generation and motif residue indices and sequence lengths from the parent

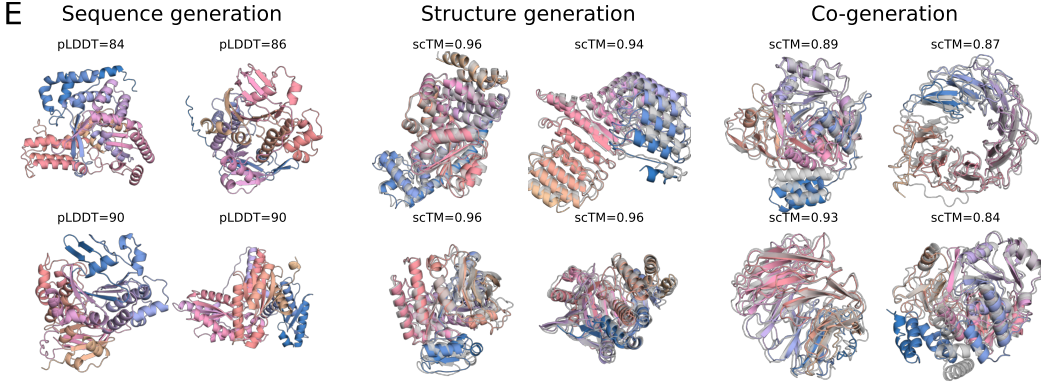


Figure 5: Overview of ProDiT and unconditional generation (continued). **(E)** Selected samples from ProDiT of length 500 under each generation protocol, labeled with the corresponding pLDDT or scTM metrics. For structure- and co-generation, the ESMFold refolded structure is superimposed in grey. RFDiff: RFDiffusion; ProtGen: ProteinGenerator.

PDB. For carbonic anhydrase, we place the EF hand motif at positions 125–136 (monotonic indexing), whereas for lysozyme we randomly place the EF hand at a random non-overlapping position in each design.

To filter the designs *in silico*, we sought to identify changes that could plausibly be sufficient to disable or reduce the activity of the enzyme based on the current understanding of its catalytic mechanism. Thus, we filtered the carbonic anhydrase scaffolds based on the displacement of core catalytic residues identified in previous work. For lysozyme, we screened using the RMSD for all motif residues due to the putative importance of non-catalytic residues in substrate recognition.

B Additional Results

B.1 Recovery of Active Sites at Atomic Fidelity

To further verify the fidelity of successful function-conditioned designs, we investigated whether ProDiT generations recover known catalytic residues and binding motifs for molecular functions with available annotations. To do so, we developed a structural alignment pipeline to screen all GO-conditioned generated structures for the presence of labeled active site residues from UniProtKB entries with the corresponding GO term (**Methods**). Briefly, we performed a global structural alignment between successful designs and AlphaFoldDB structures with ≥ 2 labeled active site residues, and filtered for designs with 100% residue identity and $< 1\text{\AA}$ RMSD for those residues. Although this pipeline is limited by the under-annotation of native active site residues in UniProtKB (across GO terms, the median percentage of structures that are sufficiently annotated is 0.23%), we found successful hits for 45 GO terms (Fig. S10, Tab. S2). In Fig. 7, we highlight two exemplar case studies that demonstrate ProDiT’s high-fidelity generation of enzyme active sites. We superimpose the generated structures against relevant PDB structures (aligned on the active site) to highlight the positioning and orientation of key residues relative to co-crystallized cofactors and substrates.

We first present a generated protein conditioned on GO:0004030, which corresponds to aldehyde dehydrogenase [NAD(P)+] activity. Aldehyde dehydrogenases catalyze the [NAD(P)+]-dependent oxidation of aldehydes to carboxylic acids and play key roles in detoxification, biosynthetic processes, antioxidant defense, and cellular regulation [3]. The generated design is aligned with the PDB structure of 1BPW—a betaine aldehyde dehydrogenase with NAD⁺ co-crystallized in the active site (Fig. 7A). The active site residues are generated with correct orientation, achieving an all-atom RMSD of 0.41 \AA (Fig. 7B,C). Furthermore, the generated protein also conserves the unique NAD⁺ binding motif that distinguishes aldehyde dehydrogenases from closely related alcohol dehydrogenases (e.g. Trp165, Asn166, Pro168, and Lys189 in the Rossmann fold) [20]. Strikingly, the sequence identity between the generated protein and 1BPW decreases with distance from the active site (Fig. 7D), indicating low overall homology (45% sequence identity).

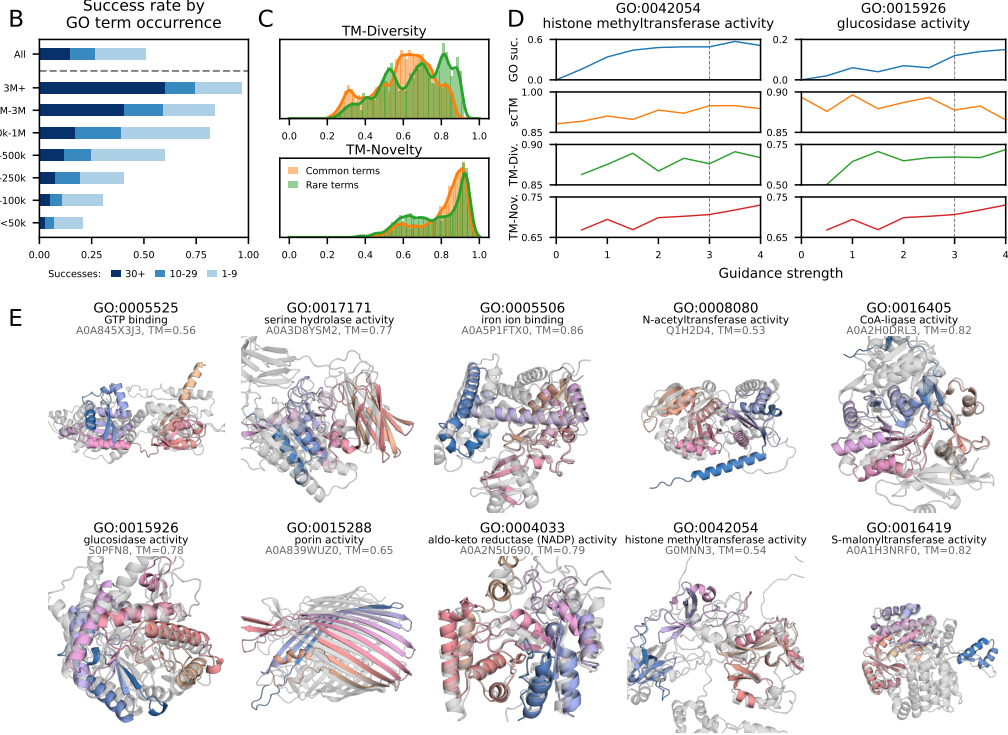


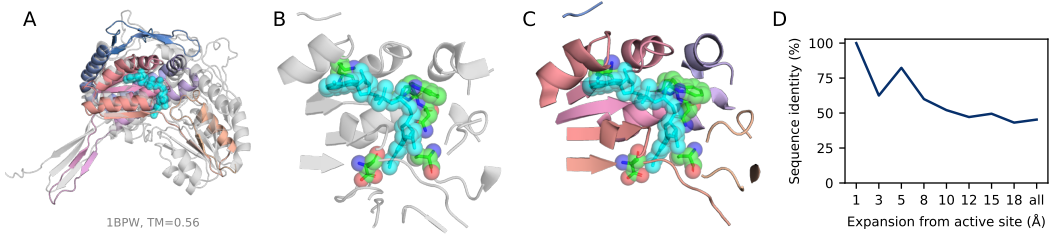
Figure 6: *In silico* validation of molecular function conditioning (continued). (B) Proportion of GO terms with different numbers of successful designs, stratified by frequency of GO term occurrence. In total, 465 terms have at least one success. **(C)** Distribution of TM-score diversity (between successful designs with the same GO term conditioning) and novelty (between designs and the most similar AlphaFoldDB entry with the same GO term) for common and rare GO terms, using a frequency cutoff of 500k. Novelty is computed only for a subset of 169 GO terms. **(D)** Impact of classifier-free guidance (CFG) for two selected GO terms with moderate success rate. For each guidance strength setting, 100 samples are generated and the success rate, mean self-consistency TM-score (scTM), diversity, and novelty are computed. Main evaluations use a guidance strength of 3. **(E)** For selected GO terms, the most novel generation is identified and superimposed onto its closest match with the same GO term from AFDB (grey).

We next showcase a generated protein conditioned on GO:0016420, which corresponds to malonyltransferase activity. These enzymes play a central role in the fatty acid biosynthesis pathway by catalyzing the transfer of a malonyl group from malonyl-CoA to the acyl carrier protein. We aligned the generated design to the holo-crystal structure of a malonyltransferase from *E. coli* (PDB ID: 2G2Z), which includes malonic semialdehyde (a substrate analogue) and CoA co-crystallized in the active site (Fig. 7E). The design not only recapitulates the conserved catalytic residues (Ser92 and His201; 0.23 Å RMSD) positioned to coordinate the substrate, but also preserves the topology of the malonyl-CoA binding pocket (Fig. 7F,G). Notably, residues critical for recognition of the malonyl carboxylate (Arg117), formation of the oxyanion hole (Gln11) [26] and binding of the CoA cofactor are all conserved. Nevertheless, the generated protein has only 41% sequence identity with the reference, with identical residues concentrated near the active site (Fig. 7H).

These case studies highlight ProDiT's ability to co-generate protein sequences and structures that preserve key catalytic residues and cofactor binding sites for diverse predicted enzymatic functions. We expect that for native functions not covered by existing GO term annotations, the overall algorithm of labeling homologous sequences and tuning the model on this additional "GO-term" label should also lead to the co-generation of novel sequences and structures that preserve essential functional residues.

Structural alignment for aldehyde dehydrogenase

GO:0004030 (aldehyde dehydrogenase [NAD(P)+] activity)



Structural alignment for malonyltransferase

GO:0016420 (malonyltransferase activity)

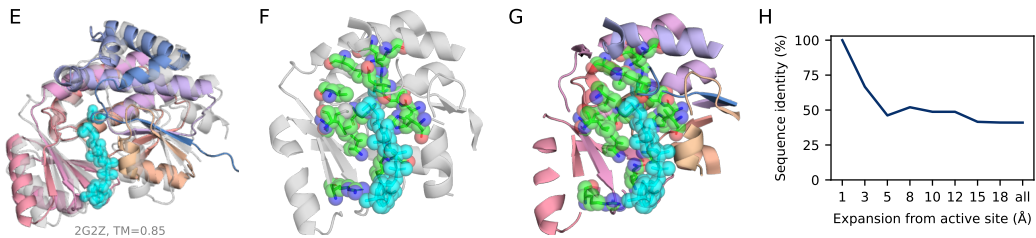


Figure 7: Validation of functional conditioning via structural alignment. (A) We superimpose a protein generated from ProDiT conditioned on aldehyde dehydrogenase [NAD(P)+] activity (GO:0004030) with PDB 1BPW, a betaine aldehyde dehydrogenase (grey), and its co-crystallized NAD⁺ cofactor (cyan). (B) View of the 10 Å neighborhood of the active site in the reference protein, 1BPW. The active site residues (E263, C297) as well as key residues in the NAD⁺ binding motif (W165, N166, P168, K189) are highlighted. (C) View of the aligned 10 Å neighborhood of the active site in the generated design. The active site and NAD⁺ binding site residues are preserved and correctly oriented. (D) Sequence identity versus distance from active site for 1BPW and the generated design. (E) We similarly superimpose a protein generation conditioned on malonyltransferase activity (GO:0016420) with PDB 2G2Z (grey), an *E. coli* malonyltransferase. The co-crystallized malonic semialdehyde and CoA ligands are also shown (cyan). (F) View of the 10 Å neighborhood of the active site in the reference protein, 2G2Z. The active site residues (S92, H201) as well as key residues in the malonyl-CoA binding motif (R117, R190, N162, Q11, Q166, Q63, H201, H91, L194, M121, M132, S92, V168, V196, V280) are highlighted. (G) View of the aligned 10 Å neighborhood of the active site in the generated design. The active site and malonyl-CoA binding site residues are preserved and correctly oriented. (H) Sequence identity versus distance from active site for 2G2Z and the generated design.

B.2 Carbonic anhydrase motif

Carbonic anhydrases catalyze the interconversion of carbon dioxide and bicarbonate (EC 4.2.1.1). This function is essential for acid-base homeostasis and is widely studied for its catalytic efficiency and potential utility in carbon capture technologies [7]. The catalytic mechanism involves a critically positioned threonine residue (Thr199) which accepts a hydrogen bond from a zinc-coordinated hydroxide ion positioned for nucleophilic attack of the substrate carbon dioxide [35, 40]. In our selected carbonic anhydrase scaffold (Fig. 4I–P), the catalytic residues are scaffolded with subatomic-level accuracy in the unbound state (0.15 Å RMSD), but calcium binding shifts the threonine hydroxyl group by ~1.04 Å in the direction of the activated hydroxide ion. This would competitively displace the Zn²⁺ coordination site occupied by the activated hydroxide nucleophile, preventing the hydration of carbon dioxide (Fig. 4M,N).

C Supplementary Figures and Tables

Figs. S1, S2, S3 show additional results, broken down by protein length, on the success rates, pLDDT, and scTM of ProDiT and baselines in unconditional sequence generation, unconditional

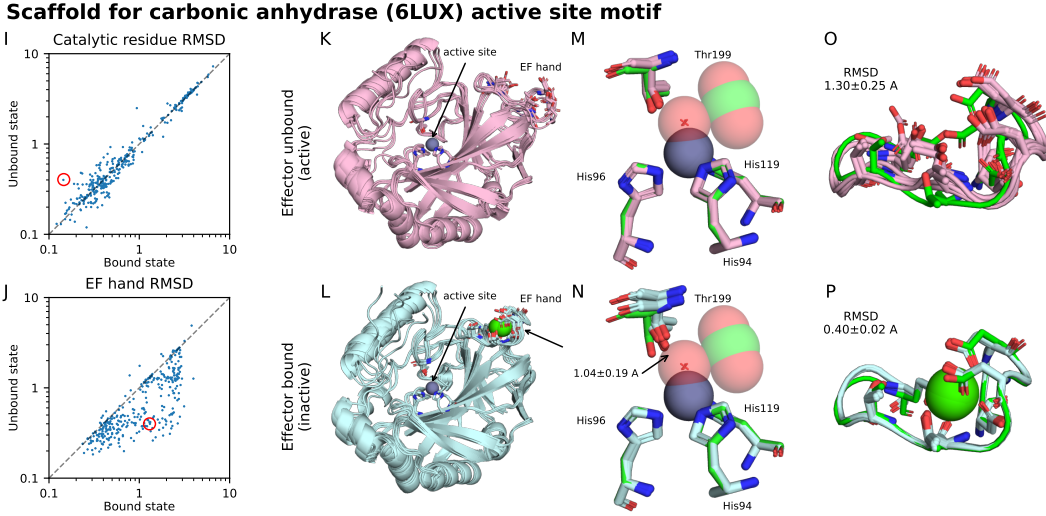


Figure 8: **In silico validation of conformation switching designs** (continued). **(I–P)** Similar analyses for the designed carbonic anhydrase active site scaffolds. **(M,N)** Active state geometry in the bound and unbound states, showing the carbon dioxide substrate, zinc cofactor, and nucleophilic hydroxide. Note the change in orientation of the catalytic residue Thr199 (full motif shown in Fig S13,S14). We report the mean and standard deviation of the displacement of the hydroxyl oxygen. Native motif colored in green in all subfigures.

structure generation, and co-generation, respectively. Fig. S4 shows similar results for structure generation and co-generation by scRMSD.

Fig. S5 compares the scTM and scRMSD of unconditional structure generation with ProDiT when inverse folding with 8x ProteinMPNN sequences versus inverse folding with ProDiT. We note that conditional generations with GO terms use ProDiT for inverse folding. Due to degraded performance, we also explore structure generation with $\nu = 0$, which produces more designable structures. We use $\nu = 0$ and inverse folding with ProDiT for GO term conditioning.

Figs. S6, S7, and S8 show diversity metrics, broken down by protein length, for sequence generation, structure generation, and co-generation respectively. In particular, TM-diversity (all) pools together all pairwise TM-scores within generations of the same length, i.e., the violinplot is a density estimator over 9900 TM-scores per protein length. On the other hand, TM-diversity (max) assigns $\max_{i \neq j} TM_{i,j}$ to be the diversity of generation i . All TM-scores are computed with TMalign.

All violin plots show the mean and inter-quartile range. Unless otherwise noted, all metrics and evaluation procedures follow their definitions in the main text.

Figs. S9 and S10 show statistics from the structural alignment pipeline for function-conditioned design.

Figs. S11 and S12 show the full lysozyme active site motif and the individual structure predictions for the selected scaffold in the bound and unbound state, along with full motif RMSDs. Figs. S13 and S14 show similar structures for the lysozyme active site motif and scaffold.

Table S1 lists the success rates, scTM, TM-diversity, and TM-novelty (when available) for all 915 GO terms evaluated for function conditioning. Table S2 provides additional results for 45 GO terms with successful structural alignment hits.

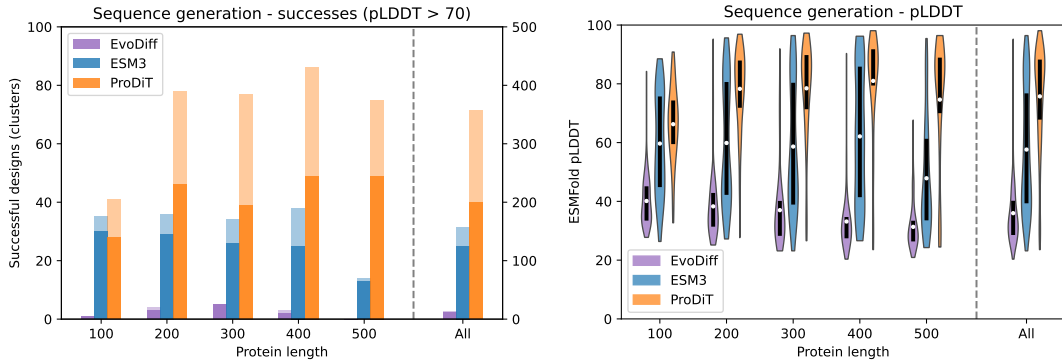


Figure S1: Success rates and ESMFold pLDDT for unconditional sequence generation.

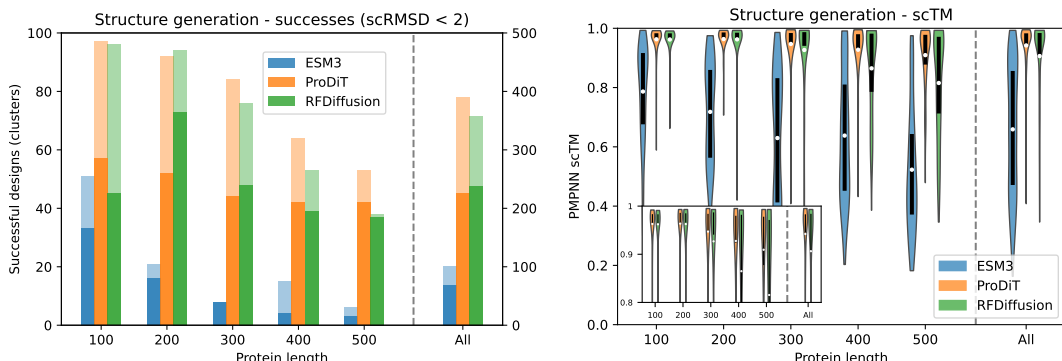


Figure S2: Success rates and scTM for unconditional structure generation.

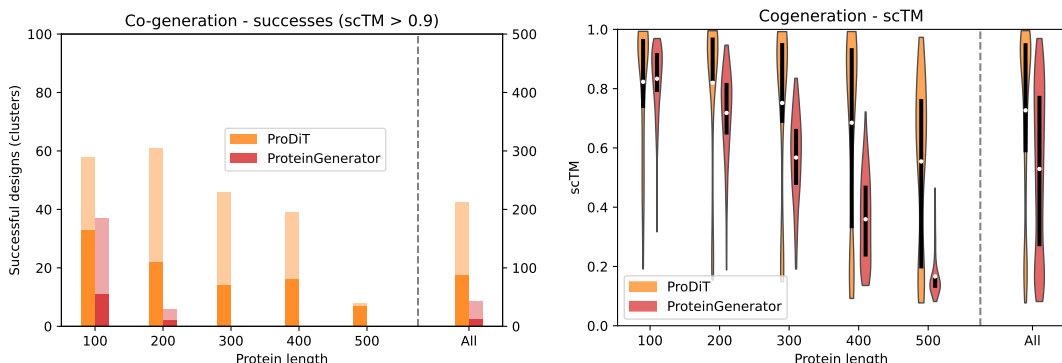


Figure S3: Success rates and scTM for sequence-structure co-generation.

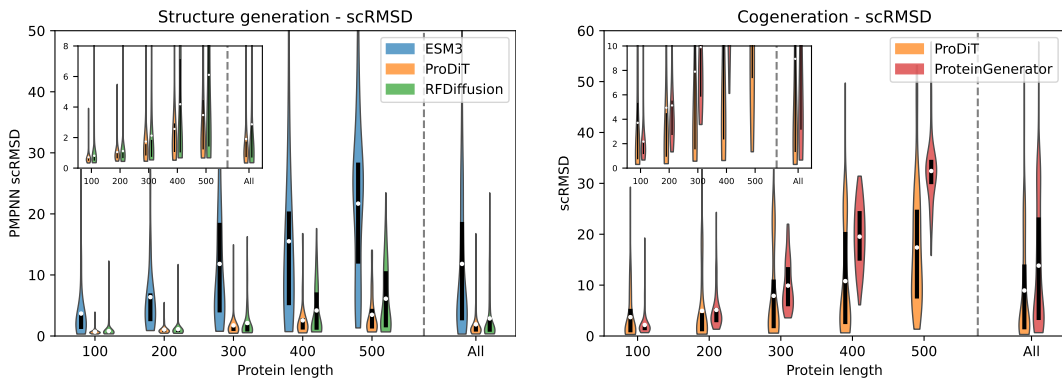


Figure S4: scRMSD for unconditional structure generation and sequence-structure co-generation

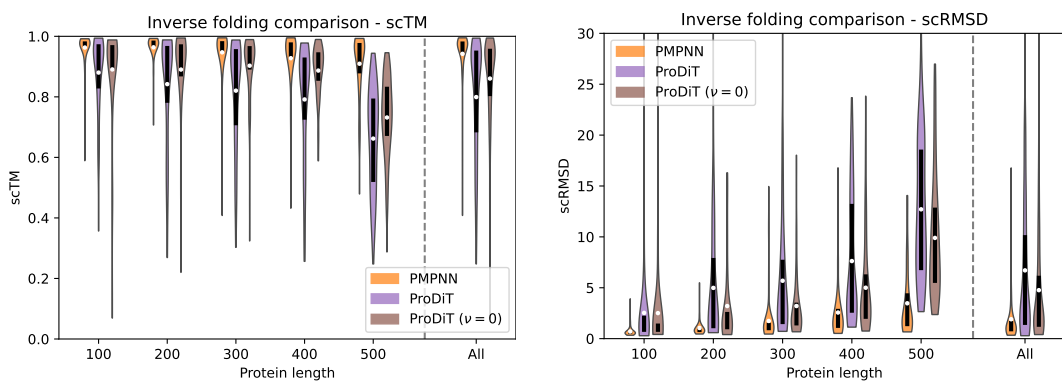


Figure S5: Comparison of inverse folding with ProteinMPNN vs ProDiT in structure generation.

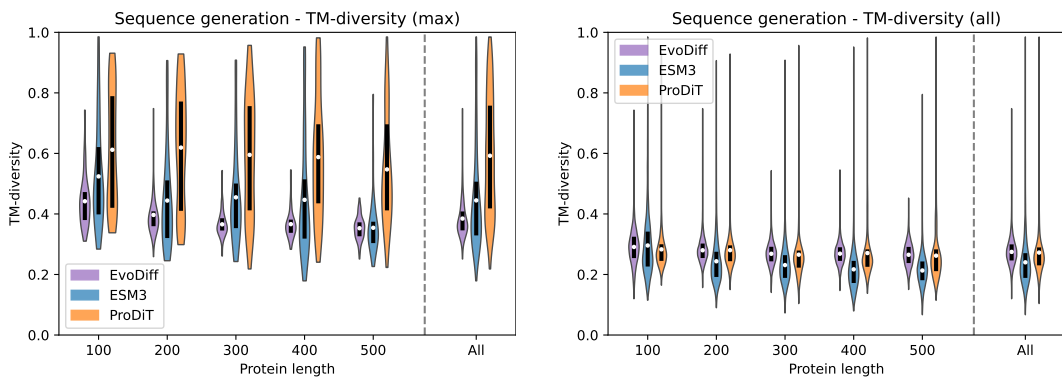


Figure S6: Diversity metrics for sequence generation. Lower TM-score means higher diversity.

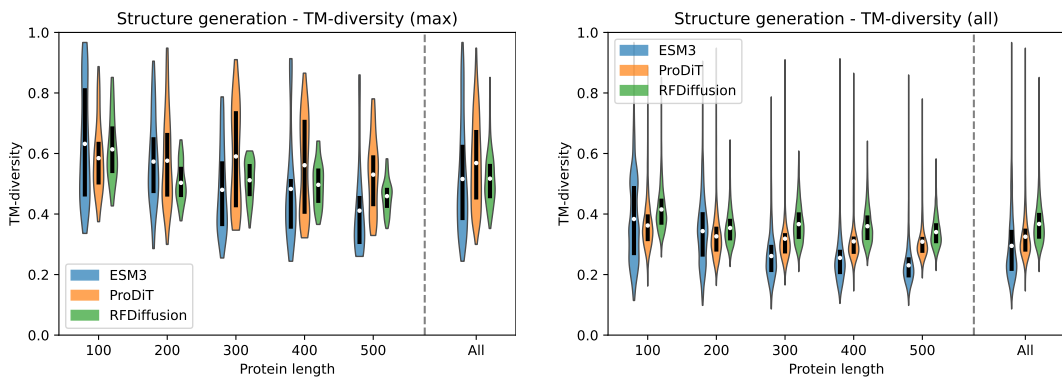


Figure S7: Diversity metrics for structure generation. Lower TM-score means higher diversity.

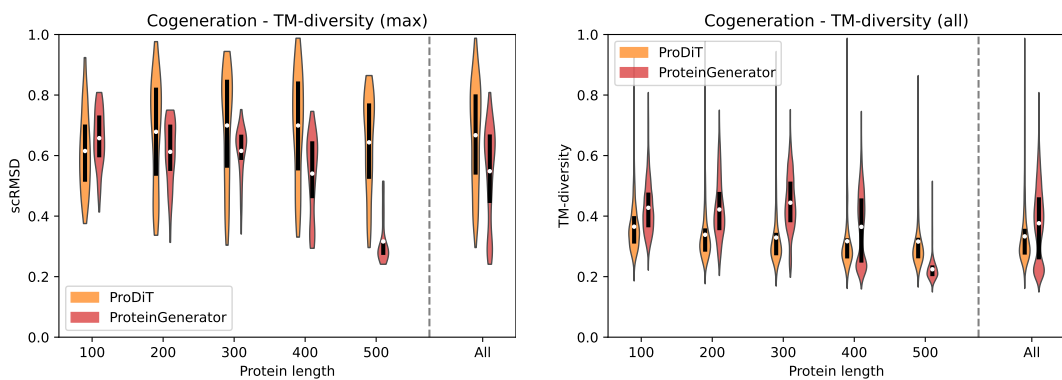


Figure S8: Diversity metrics for co-generation. Lower TM-score means higher diversity.

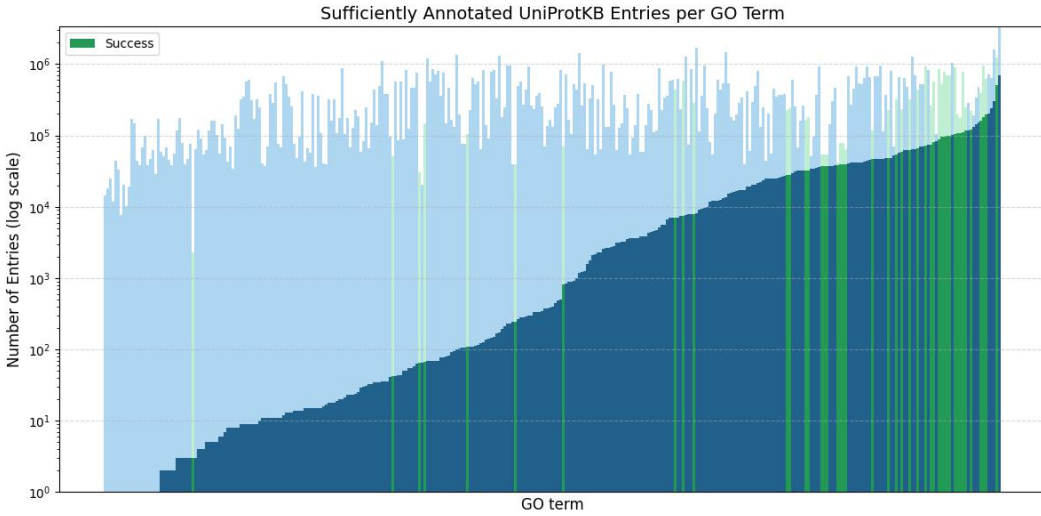


Figure S9: GO terms by number of sufficiently annotated UniProtKB entries, i.e., active sites with ≥ 2 residues. 337 GO terms are analyzed in total, out of 465 with successful ProDiT designs. Across GO terms, the median percentage of sufficiently annotated entries is 0.23%. 10 terms have zero annotated entries, and 132 terms have < 100 annotated entries. Light bars indicate the number of total entries. GO terms with successful hits in our structural alignment pipeline (Methods) are highlighted in green.

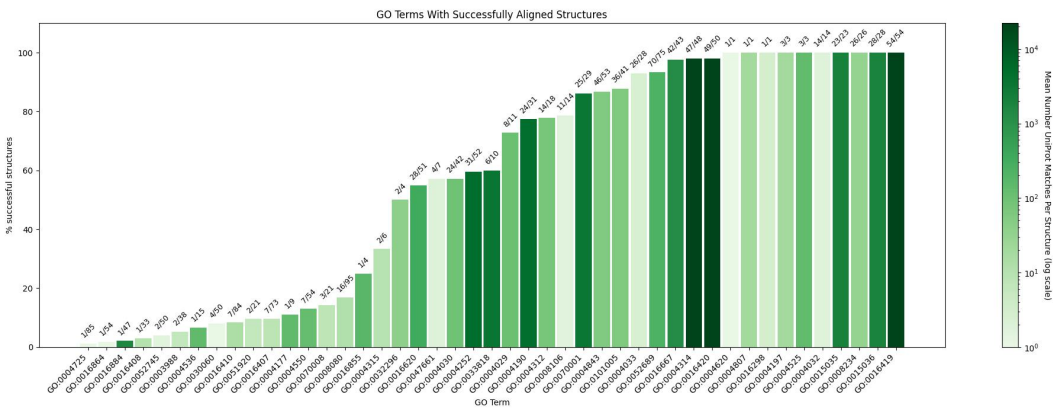


Figure S10: Statistics of GO terms with successful hits from the structural alignment pipeline (45 terms). Bars are labeled with the number of successfully aligned ProDiT generations out of total successful ProDiT generations, with the bar height indicating the percentage. The bar color indicates the mean number of matching UniProtKB entries per successful design. While most GO terms matched with a few entries (median 19), a few terms exceeded 20,000 aligned hits per design.

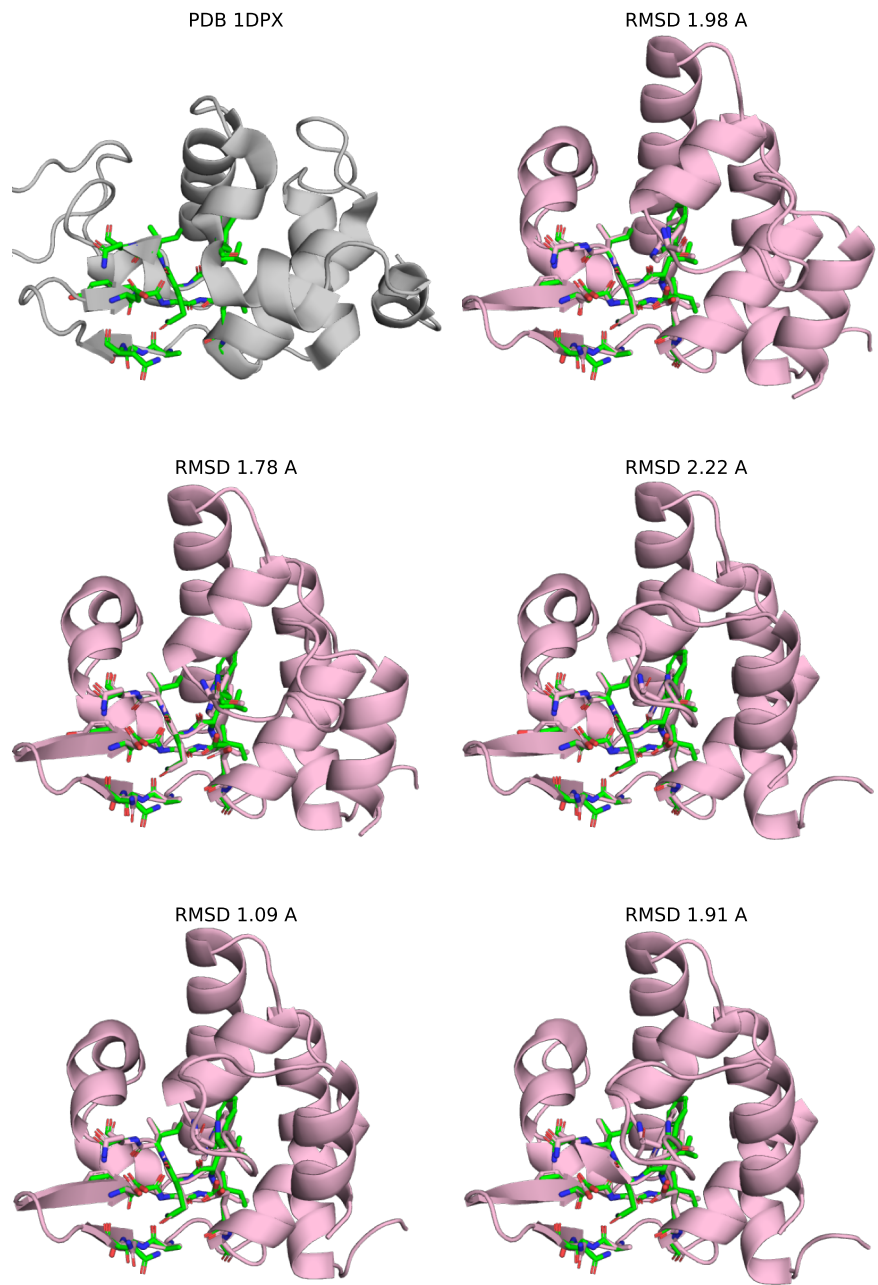


Figure S11: Unbound states of the lysozyme motif scaffold. Active site motif of lysozyme shown within PDB 1DPX (top left). The remaining structures show the five Chai-1 structure predictions without the calcium effector. The RMSD C α RMSD across all motif residues is listed.

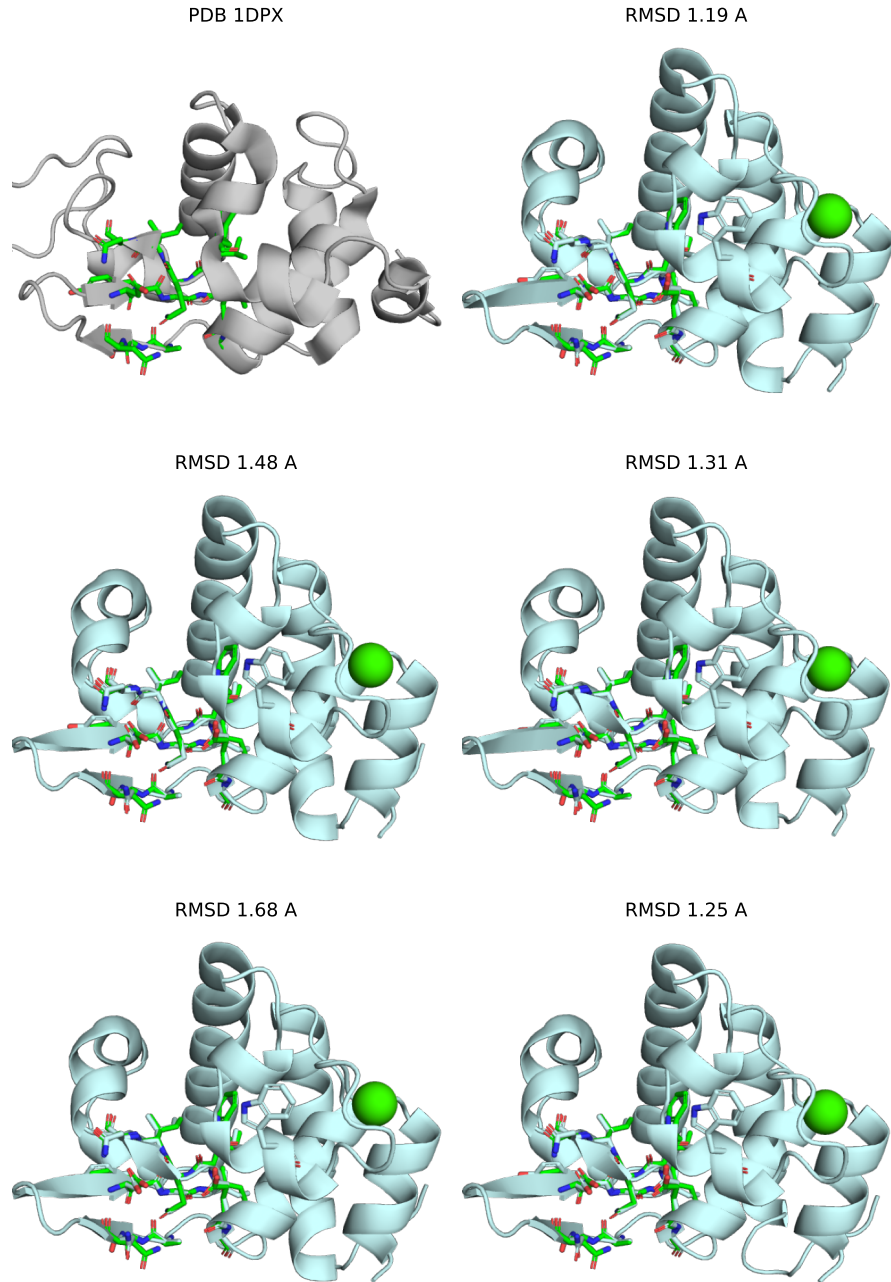


Figure S12: **Bound states of the lysozyme motif scaffold.** See previous caption.

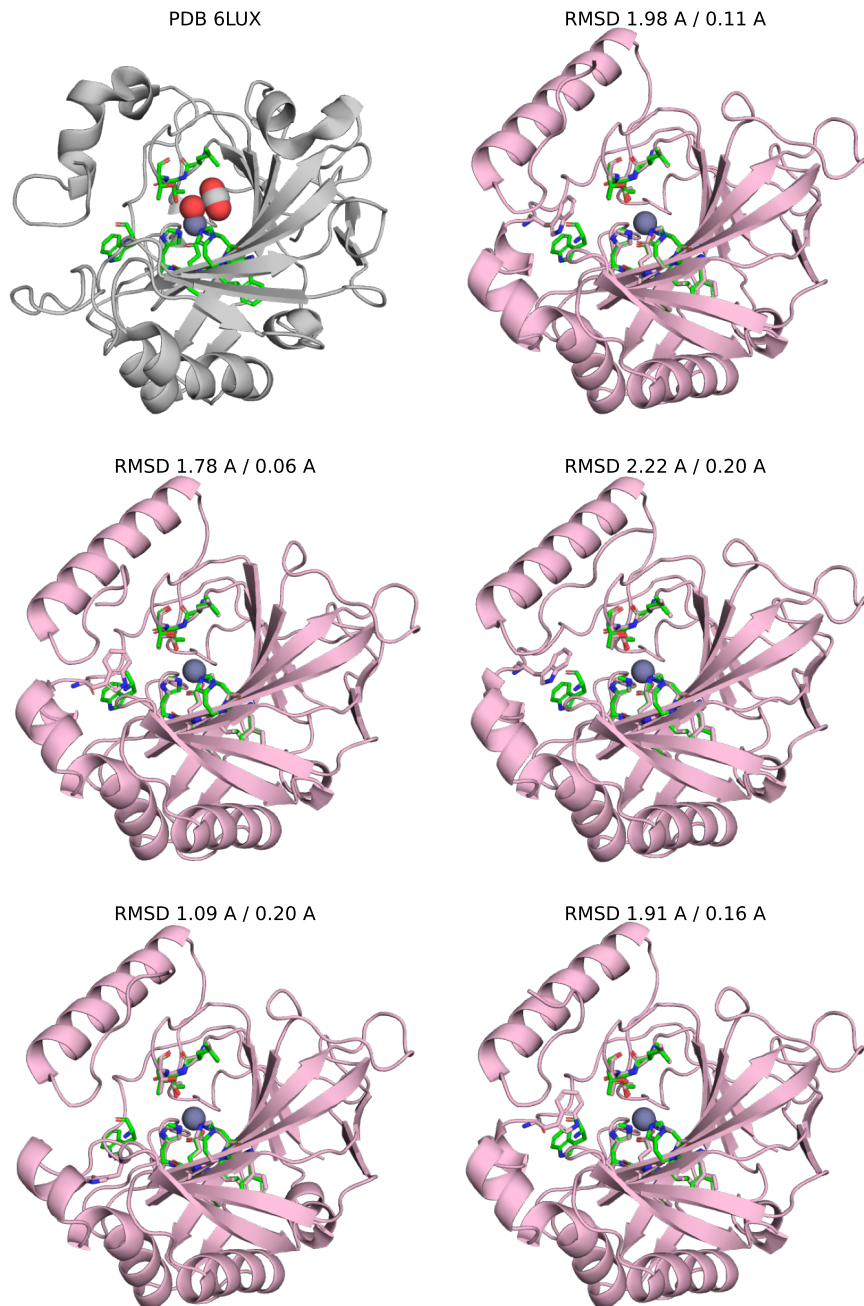


Figure S13: Unbound states of the carbonic anhydrase motif scaffold. Active site motif of carbonic anhydrase shown within PDB 6LUX (top left), with zinc cofactor and hydroxide and carbon dioxide substrates shown. The remaining structures show the five Chai-1 structure predictions without the calcium effector. The first RMSD listed is the $C\alpha$ RMSD across all motif residues. These are somewhat larger than typical cutoff of 1 Å and we found it was dominated by the placement of a tryptophan residue (left) whose impact on catalytic activity was unclear. Thus, we filtered based on $C\alpha$ RMSD of the four catalytic residues (second RMSD listed).

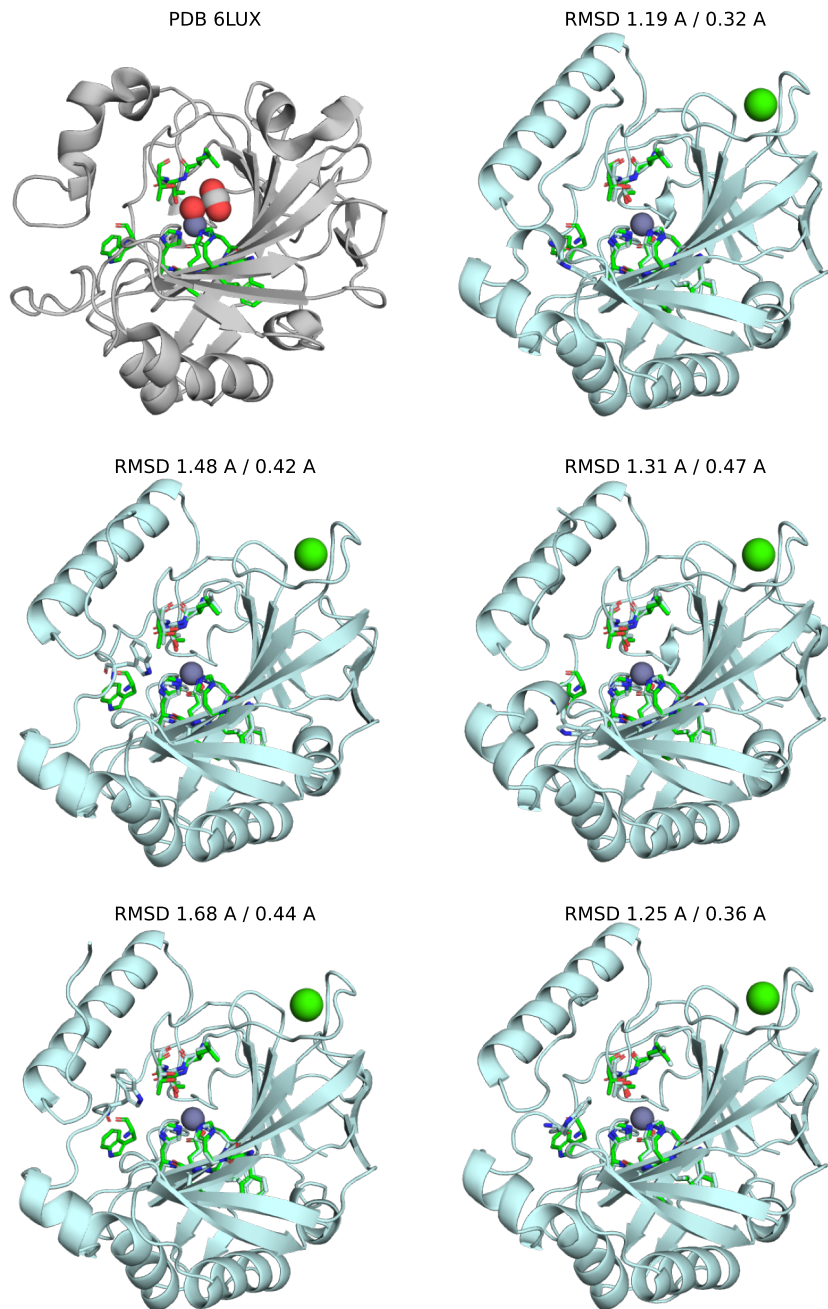


Figure S14: **Bound states of the carbonic anhydrase motif scaffold.** See previous caption.

Table S1: Descriptions and results for all 915 evaluated molecular function GO terms.

Term	Description	Occurrences	Successes	scTM	TM-diversity	TM-novelty (min)
GO:0017076	purine nucleotide binding	22956413	97	0.93	0.63	
GO:0097367	carbohydrate derivative binding	22382726	96	0.92	0.48	
GO:0032553	ribonucleotide binding	21512585	98	0.92	0.56	
GO:0032555	purine ribonucleotide binding	20786702	97	0.92	0.52	
GO:0030554	adenyl nucleotide binding	20626611	98	0.92	0.50	
GO:0035639	purine ribonucleoside triphosphate binding	20495784	99	0.92	0.49	
GO:0032559	adenyl ribonucleotide binding	18459894	100	0.92	0.52	
GO:0005524	ATP binding	18273940	97	0.92	0.48	
GO:0005215	transporter activity	17136396	98	0.93	0.52	
GO:0003677	DNA binding	16963614	67	0.85	0.57	
GO:0022857	transmembrane transporter activity	16898359	93	0.91	0.56	
GO:00140096	catalytic activity, acting on a protein	14398009	63	0.89	0.60	
GO:0016772	transferase activity, transferring phosphorus-containing groups	12146957	93	0.95	0.68	
GO:0003723	RNA binding	9077378	12	0.86	0.29	
GO:0016817	hydrolase activity, acting on acid anhydrides	8859070	64	0.88	0.49	
GO:0016818	hydrolase activity, acting on acid anhydrides, in phosphorus-containing anhydrid...	8811641	63	0.90	0.53	
GO:0016462	pyrophosphatase activity	8727052	45	0.88	0.52	
GO:0016788	hydrolase activity, acting on ester bonds	8569359	10	0.89	0.49	
GO:0046914	transition metal ion binding	7929417	6	0.76	0.45	
GO:0017111	nucleoside-triphosphatase activity	7827489	60	0.87	0.50	
GO:00410110	transcription regulator activity	7808154	66	0.67	0.37	
GO:0022804	active transmembrane transporter activity	7645552	39	0.89	0.42	
GO:0016301	kinase activity	7580968	91	0.95	0.69	
GO:0015075	ion transmembrane transporter activity	7337937	35	0.79	0.39	
GO:0015318	inorganic molecular entity transmembrane transporter activity	7243753	7	0.79	0.34	
GO:0003700	DNA-binding transcription factor activity	7091981	69	0.70	0.38	
GO:0008324	cation transmembrane transporter activity	6718093	5	0.81	0.38	
GO:0022890	inorganic cation transmembrane transporter activity	6404986	2	0.76	0.25	
GO:0008233	peptidase activity	6259124	32	0.86	0.43	
GO:0016887	ATPase activity	6242595	52	0.87	0.53	
GO:0140098	catalytic activity, acting on RNA	6210175	11	0.73	0.35	
GO:0016829	lyase activity	6098165	14	0.89	0.63	
GO:0016853	isomerase activity	6066403	2	0.93	0.82	
GO:0016773	phosphotransferase activity, alcohol group as acceptor	5777744	100	0.95	0.81	
GO:0015399	primary active transmembrane transporter activity	5615335	21	0.89	0.57	
GO:0016874	ligase activity	5509331	23	0.90	0.50	
GO:0043565	sequence-specific DNA binding	5029292	7	0.76	0.43	
GO:0140097	catalytic activity, acting on DNA	5011076	12	0.85	0.38	
GO:0005198	structural molecule activity	4966114	35	0.66	0.31	
GO:0016746	transf erase activity, transferring acyl groups	4894433	65	0.84	0.66	
GO:0009055	electron transfer activity	4656696	13	0.56	0.36	
GO:0015078	proton transmembrane transporter activity	4585439	2	0.59	0.32	
GO:0008270	zinc ion binding	4544060	1	0.80		
GO:0098772	molecular function regulator	4433343	2	0.79	0.60	
GO:0016741	transferase activity, transferring one-carbon groups	4286583	99	0.91	0.65	
GO:0004672	protein kinase activity	3988854	97	0.93	0.78	
GO:0022853	active ion transmembrane transporter activity	3958268	0	0.83		
GO:0004518	nuclease activity	3954313	33	0.83	0.46	
GO:0046906	tetrapyrrole binding	3931047	33	0.67	0.38	
GO:0016779	nucleotidyltransferase activity	3901657	32	0.86	0.41	
GO:0003690	double-stranded DNA binding	3804794	1	0.88		
GO:0008168	methyltransferase activity	3800185	99	0.92	0.66	
GO:0051540	metal cluster binding	3667718	96	0.94	0.73	
GO:0051536	iron-sulfur cluster binding	3666092	98	0.95	0.73	
GO:0016757	transf erase activity, transferring glycosyl groups	3572759	17	0.93	0.55	
GO:0020037	heme binding	3537432	34	0.65	0.41	
GO:1990837	sequence-specific double-stranded DNA binding	3373045	3	0.76	0.36	
GO:0003735	structural constituent of ribosome	3325740	37	0.50	0.26	
GO:0016747	transf erase activity, transferring acyl groups other than amino-acyl groups	3319577	72	0.84	0.66	
GO:0004175	endopeptidase activity	3263101	6	0.89	0.54	
GO:0001067	regulatory region nucleic acid binding	3225086	0	0.77		
GO:0000976	transcription regulatory region sequence-specific DNA binding	3224990	2	0.78	0.59	
GO:0000287	magnesium ion binding	3103773	6	0.92	0.51	
GO:0016810	hydrolase activity, acting on carbon-nitrogen (but not peptide) bonds	2994620	12	0.86	0.59	
GO:0016614	oxidoreductase activity, acting on CH-OH group of donors	2922896	20	0.89	0.48	
GO:0042578	phosphoric ester hydrolase activity	2756712	10	0.88	0.49	
GO:0140101	catalytic activity, acting on a tRNA	2724981	36	0.80	0.42	
GO:0016798	hydrolase activity, acting on glycosyl bonds	2679691	14	0.87	0.53	
GO:0019842	vitamin binding	2651082	83	0.85	0.65	
GO:0060089	molecular transducer activity	2646736	92	0.94	0.83	
GO:0004519	endonuclease activity	2573275	15	0.77	0.38	
GO:0016616	oxidoreductase activity, acting on the CH-OH group of donors, NAD or NADP as acc...	2569384	69	0.93	0.65	
GO:0019001	guanyl nucleotide binding	2476666	94	0.82	0.56	
GO:0032561	guanyl ribonucleotide binding	2474301	86	0.83	0.57	
GO:0050660	flavin adenine dinucleotide binding	2388837	36	0.89	0.43	
GO:0005525	GTP binding	2359411	86	0.83	0.57	0.71 (0.56)
GO:0022803	passive transmembrane transporter activity	2300712	37	0.77	0.67	
GO:0015267	channel activity	2300711	42	0.79	0.61	
GO:0042626	ATPase-coupled transmembrane transporter activity	2295752	22	0.89	0.58	
GO:0016835	carbon-oxygen lyase activity	2229362	5	0.90	0.50	
GO:0030234	enzyme regulator activity	2103061	4	0.89	0.49	
GO:0016879	ligase activity, forming carbon-nitrogen bonds	2095688	23	0.91	0.55	
GO:0019843	rRNA binding	2078018	18	0.53	0.25	
GO:0051539	4 iron, 4 sulfur cluster binding	2074241	95	0.93	0.72	
GO:0004553	hydrolase activity, hydrolyzing O-glycosyl compounds	2051554	15	0.88	0.57	
GO:0016830	carbon-carbon lyase activity	2051524	32	0.96	0.70	
GO:0016791	phosphatase activity	2048037	49	0.88	0.76	
GO:0016675	oxidoreductase activity, acting on a heme group of donors	2042281	0	0.89		

Term	Description	Occurrences	Successes	scTM	TM-diversity	TM-novelty (min)
GO:0008757	S-adenosylmethionine-dependent methyltransferase activity	2032461	15	0.92	0.67	
GO:0004129	cytochrome-c oxidase activity	2029875	1	0.84		
GO:0008237	metallopeptidase activity	2014105	10	0.87	0.49	
GO:0046873	metal ion transmembrane transporter activity	1922269	0	0.84		
GO:0015291	secondary active transmembrane transporter activity	1908900	45	0.89	0.40	0.84 (0.44)
GO:0044877	protein-containing complex binding	1890539	0	0.90		
GO:0017171	serine hydrolase activity	1870912	65	0.91	0.63	0.89 (0.77)
GO:0008236	serine-type peptidase activity	1852427	61	0.91	0.71	0.90 (0.77)
GO:0005506	iron ion binding	1849327	51	0.89	0.67	0.91 (0.86)
GO:0005216	ion channel activity	1815831	2	0.72	0.26	
GO:0038023	signaling receptor activity	1811055	93	0.92	0.82	0.89 (0.59)
GO:0004386	helicase activity	1783635	69	0.88	0.59	0.83 (0.62)
GO:0016836	hydro-lyase activity	1732784	0	0.80		
GO:0009981	DNA-binding transcription factor activity, RNA polymerase II-specific	1725696	4	0.84	0.38	
GO:0140299	small molecule sensor activity	1718536	52	0.74	0.61	0.82 (0.60)
GO:0070279	vitamin B6 binding	1696410	84	0.83	0.66	0.81 (0.61)
GO:0030170	pyridoxal phosphate binding	1696403	87	0.84	0.64	0.81 (0.60)
GO:0016705	oxidoreductase activity, acting on paired donors, with incorporation or reductio...	1673658	50	0.92	0.66	0.91 (0.80)
GO:0004497	monooxygenase activity	1672575	73	0.93	0.64	0.91 (0.80)
GO:0016651	oxidoreductase activity, acting on NAD(P)H	1671443	22	0.91	0.81	0.91 (0.83)
GO:0004674	protein serine/threonine kinase activity	1649792	97	0.95	0.80	0.88 (0.74)
GO:0008094	DNA-dependent ATPase activity	1634241	3	0.88	0.79	
GO:0016758	transf erase activity, transferring hexosyl groups	1614240	17	0.91	0.69	0.88 (0.73)
GO:0016775	phosphotransferase activity, nitrogenous group as acceptor	1566284	53	0.73	0.59	0.81 (0.55)
GO:0003924	GTPase activity	1553656	33	0.83	0.55	0.69 (0.58)
GO:0008238	exopeptidase activity	1546233	5	0.89	0.52	
GO:0016765	transf erase activity, transferring alkyl or aryl (other than methyl) groups	1511695	1	0.96		
GO:0004673	protein histidine kinase activity	1506423	56	0.74	0.62	0.83 (0.62)
GO:0016627	oxidoreductase activity, acting on the CH-CH group of donors	1453300	1	0.85		
GO:0000155	phosphorelay sensor kinase activity	1443870	49	0.76	0.63	0.82 (0.62)
GO:0004888	transmembrane signaling receptor activity	1433020	88	0.92	0.81	0.89 (0.53)
GO:0009977	RNA polymerase II transcription regulatory region sequence-specific DNA binding	1427564	7	0.74	0.65	
GO:0008092	cytoskeletal protein binding	1400761	4	0.85	0.58	
GO:0051287	NAD binding	1387693	68	0.94	0.64	0.90 (0.75)
GO:0008514	organic anion transmembrane transporter activity	1349918	0	0.92		
GO:0140359	ABC-type transporter activity	1347792	1	0.89		
GO:0016875	ligase activity, forming carbon-oxygen bonds	1343584	42	0.81	0.44	0.80 (0.46)
GO:0004812	aminoacyl-tRNA ligase activity	1343583	34	0.78	0.46	0.81 (0.49)
GO:0004540	ribonuclease activity	1338388	12	0.67	0.46	0.64 (0.51)
GO:0016811	hydrolase activity, acting on carbon-nitrogen (but not peptide) bonds, in linear...	1306946	9	0.78	0.37	
GO:0005509	calcium ion binding	1274794	3	0.79	0.32	
GO:0019899	enzyme binding	1270249	0	0.90		
GO:0016769	transferase activity, transferring nitrogenous groups	1261805	56	0.86	0.70	0.84 (0.67)
GO:0046983	protein dimerization activity	1256161	0	0.82		
GO:0000049	tRNA binding	1255859	0	0.80		
GO:0016655	oxidoreductase activity, acting on NAD(P)H, quinone or similar compound as accep...	1254605	3	0.81	0.48	
GO:0030246	carbohydrate binding	1246103	0	0.80		
GO:0008289	lipid binding	1246092	2	0.76	0.47	
GO:0009897	cis-regulatory region sequence-specific DNA binding	1241391	0	0.78		
GO:0004252	transaminase activity	1233439	40	0.86	0.69	0.83 (0.72)
GO:0004843	carboxy-lyase activity	1227333	1	0.96		
GO:0016831	exonuclease activity	1225169	13	0.83	0.46	0.68 (0.64)
GO:0004527	RNA polymerase II cis-regulatory region sequence-specific DNA binding	1212767	1	0.75		
GO:0009978	serine-type endopeptidase activity	1203621	52	0.89	0.71	0.90 (0.77)
GO:0004252	cation channel activity	1201026	5	0.71	0.31	
GO:0005261	organic acid transmembrane transporter activity	1197798	0	0.94		
GO:0005342	carboxylic acid transmembrane transporter activity	1194014	0	0.92		
GO:0046943	mRNA binding	1191978	1	0.84		
GO:0003729	DNA polymerase activity	1160534	1	0.84		
GO:0034061	oxidoreductase activity, acting on the aldehyde or oxo group of donors	1158157	26	0.89	0.51	0.87 (0.49)
GO:0016903	molecular adaptor activity	1144566	0	0.90		
GO:0060090	carboxylic ester hydrolase activity	1117280	75	0.92	0.75	0.83 (0.72)
GO:00052689	NADP binding	1108426	28	0.93	0.62	0.87 (0.64)
GO:0050661	NADH dehydrogenase activity	1068866	0	0.90		
GO:0003954	RNA methyltransferase activity	1051776	46	0.82	0.66	0.76 (0.53)
GO:0008173	acetyltransferase activity	1047779	2	0.66	0.44	
GO:0005102	signaling receptor binding	1039567	2	0.90	0.47	
GO:0004222	metalloendopeptidase activity	1032013	0	0.83		
GO:0030674	protein-macromolecule adaptor activity	992216	0	0.74		
GO:0016755	transferase activity, transferring amino-acyl groups	984696	8	0.66	0.58	
GO:0016209	antioxidant activity	978586	73	0.82	0.56	0.68 (0.49)
GO:0016407	acetyltransferase activity	962044	16	0.85	0.53	0.83 (0.53)
GO:1901681	sulfur compound binding	960603	0	0.88		
GO:0016763	transferase activity, transferring pentosyl groups	953811	1	0.54		
GO:0097747	RNA polymerase activity	935806	0	0.49		
GO:0034062	5'-3' RNA polymerase activity	930429	14	0.81	0.56	0.71 (0.58)
GO:0016866	intramolecular transferase activity	925662	0	0.79		
GO:0043021	ribonucleoprotein complex binding	902290	1	0.81		
GO:0015103	inorganic anion transmembrane transporter activity	894093	23	0.91	0.82	0.89 (0.70)
GO:0051213	dioxygenase activity	881281	43	0.60	0.43	0.54 (0.37)
GO:0016667	oxidoreductase activity, acting on a sulfur group of donors	877645	32	0.89	0.74	0.87 (0.81)
GO:0008194	UDP-glycosyltransferase activity	862098	15	0.88	0.73	0.77 (0.70)
GO:0004536	deoxyribonuclease activity	854063	9	0.67	0.48	
GO:0004521	endoribonuclease activity	849661	5	0.69	0.31	
GO:0019787	ubiquitin-like protein transferase activity	847303	51	0.90	0.62	0.91 (0.57)
GO:0016620	oxidoreductase activity, acting on the aldehyde or oxo group of donors, NAD or N...	837294	13	0.88	0.54	0.84 (0.73)
GO:0003678	DNA helicase activity	836827	2	0.93	0.85	
GO:0016782	transferase activity, transferring sulfur-containing groups	836817	0	0.83		
GO:0008137	NADH dehydrogenase (ubiquinone) activity	828247	4	0.88	0.67	
GO:0060589	nucleoside-triphosphatase regulator activity	828247	6	0.88	0.41	
GO:0030695	GTPase regulator activity					

Term	Description	Occurrences	Successes	scTM	TM-diversity	TM-novelty (min)
GO:0051537	2 iron, 2 sulfur cluster binding	821490	9	0.72	0.43	
GO:0022836	gated channel activity	816718	4	0.67	0.31	
GO:0043022	ribosome binding	813766	0	0.72		
GO:0051082	unfolded protein binding	798764	16	0.69	0.36	0.62 (0.46)
GO:0015293	symporter activity	797934	20	0.91	0.68	0.86 (0.73)
GO:0008170	N-methyltransferase activity	797048	62	0.85	0.52	0.76 (0.46)
GO:0004842	ubiquitin-protein transferase activity	792861	5	0.72	0.30	
GO:0071949	FAD binding	789552	31	0.93	0.68	0.86 (0.75)
GO:0015297	antiporter activity	784942	26	0.91	0.57	0.87 (0.75)
GO:0016854	racemase and epimerase activity	781790	6	0.90	0.62	
GO:0016298	lipase activity	756077	1	0.90		
GO:0004930	G protein-coupled receptor activity	739118	92	0.94	0.84	0.91 (0.75)
GO:0010181	FMN binding	725734	30	0.75	0.60	0.82 (0.53)
GO:0008047	enzyme activator activity	723085	1	0.85		
GO:0048038	quinone binding	720241	0	0.66		
GO:0003779	actin binding	702220	1	0.86		
GO:0004180	carboxypeptidase activity	697021	3	0.87	0.74	
GO:0008408	3'-5' exonuclease activity	695714	5	0.78	0.54	
GO:0016410	N-acyltransferase activity	685071	84	0.79	0.57	0.69 (0.52)
GO:0016881	acid-amino acid ligase activity	670208	10	0.95	0.69	
GO:0016860	intramolecular oxidoreductase activity	670193	0	0.89		
GO:0019829	ATPase-coupled cation transmembrane transporter activity	663252	28	0.76	0.52	0.79 (0.53)
GO:0004721	phosphoprotein phosphatase activity	659947	91	0.89	0.78	0.88 (0.56)
GO:0016987	sigma factor activity	655629	79	0.57	0.43	0.54 (0.38)
GO:0043177	organic acid binding	655428	4	0.83	0.60	
GO:0016684	oxidoreductase activity, acting on peroxide as acceptor	642951	23	0.79	0.65	0.84 (0.49)
GO:0031406	carboxylic acid binding	641396	3	0.87	0.55	
GO:0016877	ligase activity, forming carbon-sulfur bonds	640204	28	0.91	0.67	0.89 (0.73)
GO:0070001	aspartic-type peptidase activity	639411	28	0.92	0.75	0.89 (0.72)
GO:0004190	aspartic-type endopeptidase activity	639366	31	0.92	0.76	0.89 (0.75)
GO:0003712	transcription coregulator activity	637013	0	0.76		
GO:0005543	phospholipid binding	626473	1	0.60		
GO:0004601	peroxidase activity	623942	27	0.84	0.81	0.89 (0.78)
GO:00033218	amide binding	622759	2	0.86	0.28	
GO:0015081	sodium ion transmembrane transporter activity	620734	0	0.81		
GO:0005319	lipid transporter activity	619574	1	0.79		
GO:0000156	phosphorelay response regulator activity	618575	11	0.58	0.48	0.67 (0.50)
GO:0008234	cysteine-type peptidase activity	611038	26	0.88	0.73	0.86 (0.75)
GO:0016814	hydrolase activity, acting on carbon-nitrogen (but not peptide) bonds, in cyclic...	601834	13	0.85	0.40	0.53 (0.44)
GO:0042802	identical protein binding	599947	0	0.89		
GO:0015252	proton channel activity	597603	7	0.70	0.62	
GO:0015144	carbohydrate transmembrane transporter activity	597099	5	0.88	0.65	
GO:0003746	translation elongation factor activity	594921	7	0.76	0.54	
GO:0061659	ubiquitin-like protein ligase activity	593105	1	0.71		
GO:0140102	catalytic activity, acting on a rRNA	591267	2	0.83	0.60	
GO:0044183	protein folding chaperone	590515	6	0.74	0.60	
GO:0003887	DNA-directed DNA polymerase activity	581719	7	0.80	0.43	
GO:0008649	rRNA methyltransferase activity	581636	2	0.81	0.63	
GO:0003899	DNA-directed 5'-3' RNA polymerase activity	580828	0	0.46		
GO:0046933	proton-transporting ATP synthase activity, rotational mechanism	577013	8	0.66	0.68	
GO:0022884	macromolecule transmembrane transporter activity	573967	46	0.68	0.56	0.67 (0.46)
GO:0005507	copper ion binding	569354	57	0.80	0.67	0.81 (0.55)
GO:0015631	tubulin binding	567778	2	0.88	0.67	
GO:0046915	transition metal ion transmembrane transporter activity	564447	0	0.82		
GO:0016884	carbon-nitrogen ligase activity, with glutamine as amido-N-donor	562214	47	0.82	0.58	0.76 (0.56)
GO:0004177	aminopeptidase activity	560516	9	0.90	0.53	
GO:0004857	enzyme inhibitor activity	559708	13	0.67	0.40	0.73 (0.44)
GO:0061630	ubiquitin protein ligase activity	559277	1	0.76		
GO:0016628	oxidoreductase activity, acting on the CH-CH group of donors, NAD or NADP as acc...	555290	0	0.95		
GO:0008235	metalloexopeptidase activity	553331	0	0.94		
GO:0015079	potassium ion transmembrane transporter activity	545752	0	0.81		
GO:0008081	phosphoric diester hydrolase activity	544643	1	0.89		
GO:0016645	oxidoreductase activity, acting on the CH-NH group of donors	535656	1	0.87		
GO:0008080	N-acetyltransferase activity	530315	95	0.74	0.53	0.67 (0.53)
GO:0016780	phosphotransferase activity, for other substituted phosphate groups	529932	4	0.79	0.70	
GO:0008276	protein methyltransferase activity	527611	4	0.81	0.58	
GO:0016776	phosphotransferase activity, phosphate group as acceptor	521507	11	0.90	0.59	0.64 (0.60)
GO:0015036	disulfide oxidoreductase activity	511010	28	0.66	0.41	0.53 (0.40)
GO:0003682	chromatin binding	502923	0	0.90		
GO:0004520	endodeoxyribonuclease activity	500131	5	0.81	0.71	
GO:0016891	endonuclease activity, producing 5'-phosphomonooesters	490474	6	0.65	0.55	
GO:0016799	hydrolase activity, hydrolyzing N-glycosyl compounds	490295	0	0.91		
GO:0003697	single-stranded DNA binding	489432	0	0.78		
GO:0016859	cis-trans isomerase activity	486912	70	0.64	0.35	0.62 (0.43)
GO:0030145	manganese ion binding	486286	2	0.82	0.69	
GO:0008017	microtubule binding	486051	9	0.90	0.87	
GO:0008374	O-acyltransferase activity	482662	0	0.88		
GO:0016878	acid-thiol ligase activity	480335	31	0.90	0.74	0.91 (0.66)
GO:0016840	carbon-nitrogen lyase activity	479167	1	0.76		
GO:0016861	intramolecular oxidoreductase activity, interconverting aldoses and ketoses	476753	3	0.89	0.52	
GO:0070566	adenylyltransferase activity	470900	3	0.86	0.58	
GO:0016783	sulfurtransferase activity	462118	1	0.82		
GO:0016679	oxidoreductase activity, acting on diphenols and related substances as donors	461632	0	0.79		
GO:0051015	actin filament binding	459208	0	0.76		
GO:0019200	carbohydrate kinase activity	457830	32	0.95	0.82	0.90 (0.79)
GO:0042910	xenobiotic transmembrane transporter activity	455111	5	0.82	0.78	
GO:0003684	damaged DNA binding	454263	5	0.75	0.77	
GO:0019239	deaminase activity	452147	4	0.54	0.49	
GO:0003755	peptidyl-prolyl cis-trans isomerase activity	442470	65	0.66	0.37	0.64 (0.48)
GO:0042277	peptide binding	440930	0	0.80		

Term	Description	Occurrences	Successes	scTM	TM-diversity	TM-novelty (min)
GO:0016638	oxidoreductase activity, acting on the CH-NH2 group of donors	437700	0	0.74		
GO:0003724	RNA helicase activity	432940	51	0.88	0.71	0.89 (0.64)
GO:0019205	nucleobase-containing compound kinase activity	428538	45	0.69	0.43	0.63 (0.45)
GO:0003743	translation initiation factor activity	427712	1	0.89		
GO:0005085	guanyl-nucleotide exchange factor activity	422714	1	0.85		
GO:0061783	peptidoglycan muralytic activity	412307	7	0.69	0.38	
GO:0003774	motor activity	411820	30	0.73	0.69	0.88 (0.45)
GO:0008509	anion transmembrane transporter activity	408132	10	0.80	0.54	
GO:0016857	racemase and epimerase activity, acting on carbohydrates and derivatives	406365	2	0.95	0.93	
GO:0015562	efflux transmembrane transporter activity	401819	0	0.72		
GO:0005096	GTPase activator activity	398956	0	0.87		
GO:0030545	receptor regulator activity	398720	0	0.50		
GO:0140104	molecular carrier activity	396509	2	0.83	0.47	
GO:0018455	alcohol dehydrogenase [NAD(P)+] activity	386197	0	0.94		
GO:0042393	histone binding	384803	0	0.93		
GO:0016405	CoA-ligase activity	383092	14	0.93	0.66	0.90 (0.82)
GO:0030546	signaling receptor activator activity	382539	0	0.50		
GO:0022834	ligand-gated channel activity	380244	9	0.68	0.43	
GO:0015276	ligand-gated ion channel activity	380221	5	0.72	0.49	
GO:0048018	receptor ligand activity	379124	0	0.52		
GO:0070008	serine-type exopeptidase activity	375821	21	0.86	0.65	0.85 (0.73)
GO:0140318	protein transporter activity	375362	56	0.70	0.56	0.68 (0.54)
GO:0015035	protein disulfide oxidoreductase activity	373674	23	0.64	0.40	0.52 (0.41)
GO:0015926	glucosidase activity	373288	12	0.88	0.67	0.88 (0.78)
GO:0042887	amide transmembrane transporter activity	372597	0	0.77		
GO:0035091	phosphatidylinositol binding	372390	0	0.55		
GO:0016701	oxidoreductase activity, acting on single donors with incorporation of molecular..	371853	0	0.75		
GO:0016646	oxidoreductase activity, acting on the CH-NH group of donors, NAD or NADP as acc...	371626	0	0.64		
GO:0008320	protein transmembrane transporter activity	369556	41	0.70	0.56	0.67 (0.46)
GO:0003995	acyl-CoA dehydrogenase activity	368669	1	0.84		
GO:0004620	phospholipase activity	366350	1	0.85		
GO:0030976	thiamine pyrophosphate binding	366135	70	0.80	0.65	0.83 (0.56)
GO:0002161	aminoacyl-tRNA editing activity	363767	0	0.70		
GO:0004659	prenyltransferase activity	363634	34	0.96	0.85	0.91 (0.86)
GO:0019207	kinase regulator activity	362615	2	0.84	0.67	
GO:0016812	hydrolase activity, acting on carbon-nitrogen (but not peptide) bonds, in cyclic...	362310	0	0.88		
GO:0016790	thioester hydrolase activity	360404	1	0.91		
GO:0016832	aldehyde-lyase activity	358997	17	0.95	0.68	0.71 (0.62)
GO:0008171	O-methyltransferase activity	358278	5	0.79	0.62	
GO:0004532	exoribonuclease activity	358046	3	0.86	0.37	
GO:0016896	exoribonuclease activity, producing 5'-phosphomonoesters	356272	2	0.84	0.67	
GO:0051087	chaperone binding	355704	0	0.65		
GO:0003968	RNA-directed 5'-3' RNA polymerase activity	355397	0	0.63		
GO:0008175	tRNA methyltransferase activity	354939	0	0.83		
GO:0033293	monocarboxylic acid binding	354050	7	0.88	0.81	
GO:0022832	voltage-gated channel activity	353268	1	0.78		
GO:0005244	voltage-gated ion channel activity	348850	1	0.79		
GO:0009982	pseudouridine synthase activity	347828	12	0.80	0.59	0.72 (0.64)
GO:0016849	phosphorus-oxygen lyase activity	347026	2	0.83	0.71	
GO:0043138	3'-5' DNA helicase activity	345757	1	0.84		
GO:1901505	carbohydrate derivative transmembrane transporter activity	344573	0	0.94		
GO:0019213	deacetylase activity	344273	38	0.93	0.80	0.91 (0.82)
GO:0050839	cell adhesion molecule binding	343855	0	0.65		
GO:0019900	kinase binding	341591	0	0.86		
GO:0016725	oxidoreductase activity, acting on CH or CH2 groups	338182	0	0.81		
GO:0019887	protein kinase regulator activity	336984	4	0.86	0.74	
GO:0008121	ubiquinol-cytochrome-c reductase activity	335075	0	0.64		
GO:0004713	protein tyrosine kinase activity	334566	5	0.93	0.84	
GO:0019104	DNA N-glycosylase activity	334066	2	0.79	0.60	
GO:0004529	exodeoxyribonuclease activity	332639	0	0.90		
GO:0003916	DNA topoisomerase activity	332125	0	0.58		
GO:0022829	wide pore channel activity	329047	83	0.78	0.66	0.73 (0.64)
GO:0015085	calcium ion transmembrane transporter activity	327655	0	0.73		
GO:0004185	serine-type carboxypeptidase activity	325789	11	0.85	0.61	0.84 (0.78)
GO:0016833	oxo-acid-lyase activity	321911	4	0.92	0.68	
GO:0016744	transferase activity, transferring aldehyde or ketonic groups	320870	2	0.82	0.66	
GO:0016742	hydroxymethyl-, formyl- and related transferase activity	312014	52	0.78	0.66	0.73 (0.63)
GO:0016668	oxidoreductase activity, acting on a sulfur group of donors, NAD(P) as acceptor	308942	13	0.82	0.79	0.90 (0.86)
GO:0019901	protein kinase binding	306556	0	0.86		
GO:0016885	ligase activity, forming carbon-carbon bonds	304114	21	0.76	0.63	0.71 (0.50)
GO:0016846	carbon-sulfur lyase activity	299307	0	0.55		
GO:0016706	2-oxoglutarate-dependent dioxygenase activity	298609	25	0.93	0.83	0.90 (0.66)
GO:0016895	exodeoxyribonuclease activity, producing 5'-phosphomonoesters	296545	0	0.89		
GO:0015288	porin activity	294099	82	0.77	0.67	0.74 (0.65)
GO:0042625	ATPase-coupled ion transmembrane transporter activity	293538	17	0.73	0.49	0.39 (0.35)
GO:0044769	ATPase activity, coupled to transmembrane movement of ions, rotational mechanism ..	293538	0	0.69		
GO:0046961	proton-transporting ATPase activity, rotational mechanism	293534	0	0.68		
GO:1904680	peptide transmembrane transporter activity	289117	0	0.92		
GO:0015108	chloride transmembrane transporter activity	288037	0	0.82		
GO:0070006	metalloaminopeptidase activity	285995	1	0.85		
GO:0043531	ADP binding	284214	0	0.79		
GO:0016709	oxidoreductase activity, acting on paired donors, with incorporation or reductio...	282920	14	0.85	0.48	0.89 (0.81)
GO:0016421	CoA carboxylase activity	278143	21	0.76	0.66	0.75 (0.68)
GO:0061134	peptidase regulator activity	277655	13	0.73	0.37	0.69 (0.45)
GO:0015343	siderophore transmembrane transporter activity	277010	0	0.80		
GO:0004176	ATP-dependent peptidase activity	276609	0	0.79		
GO:0016868	intramolecular transferase activity, phosphotransferases	276230	7	0.91	0.45	
GO:0072341	modified amino acid binding	272661	1	0.86		
GO:0016702	oxidoreductase activity, acting on single donors with incorporation of molecular..	269657	0	0.73		
GO:0016774	phosphotransferase activity, carboxyl group as acceptor	269512	8	0.94	0.75	

Term	Description	Occurrences	Successes	scTM	TM-diversity	TM-novelty (min)
GO:0016841	ammonia-lyase activity	268283	0	0.75		
GO:0019238	cyclohydrolase activity	267098	0	0.72		
GO:0047429	nucleoside-triphosphate diphosphatase activity	264998	1	0.67		
GO:0004197	cysteine-type endopeptidase activity	264740	3	0.88	0.82	
GO:1901682	sulfur compound transmembrane transporter activity	264310	1	0.85		
GO:0016743	carboxyl- or carbamoyltransferase activity	264082	0	0.92		
GO:0015344	siderophore uptake transmembrane transporter activity	263969	0	0.81		
GO:0009975	transcription copressor activity	262340	0	0.78		
GO:0051920	cyclase activity	260126	0	0.82		
GO:0016597	peroxiredoxin activity	259891	21	0.60	0.41	0.57 (0.49)
GO:0031419	amino acid binding	254807	0	0.93		
GO:0004523	cobalamin binding	254366	2	0.84	0.49	
GO:0005253	RNA-DNA hybrid ribonuclease activity	254340	1	0.67		
GO:0004315	anion channel activity	254123	0	0.79		
GO:0046982	3-oxoacyl-[acyl-carrier-protein] synthase activity	250204	6	0.93	0.63	
GO:0022843	protein heterodimerization activity	249572	41	0.48	0.45	0.58 (0.35)
GO:0070403	voltage-gated cation channel activity	248850	0	0.67		
GO:0048029	NAD ⁺ binding	248521	0	0.85		
GO:0030414	monosaccharide binding	244902	5	0.84	0.66	
GO:0005516	peptidase inhibitor activity	244760	25	0.68	0.36	0.67 (0.45)
GO:0004725	calmodulin binding	244194	0	0.89		
GO:0004722	protein tyrosine phosphatase activity	243683	85	0.90	0.81	0.90 (0.59)
GO:0016408	protein serine/threonine phosphatase activity	242119	47	0.90	0.80	0.87 (0.78)
GO:0000175	C-acetyltransferase activity	241558	33	0.84	0.75	0.91 (0.79)
GO:0008658	3'-5'-exoribonuclease activity	232878	2	0.86	0.74	
GO:0005048	penicillin binding	232739	5	0.86	0.66	
GO:0005267	signal sequence binding	229591	0	0.95		
GO:0061135	potassium channel activity	227662	4	0.68	0.42	
GO:0051020	endopeptidase regulator activity	226608	21	0.73	0.42	0.73 (0.41)
GO:0101005	GTPase binding	226175	0	0.88		
GO:0016289	ubiquitinyl hydrolase activity	226115	41	0.92	0.87	0.92 (0.83)
GO:0004030	CoA hydrolase activity	225380	0	0.88		
GO:0140030	aldehyde dehydrogenase [NAD(P)+] activity	222506	42	0.92	0.81	0.95 (0.90)
GO:0046912	modification-dependent protein binding	220696	0	0.84		
GO:0031267	transf erase activity, transferring acyl groups, acyl groups converted into alkyl...	219651	0	0.79		
GO:0003918	small GTPase binding	219031	0	0.90		
GO:0016855	DNA topoisomerase type II (double strand cut, ATP-hydrolyzing) activity	218942	0	0.59		
GO:0004866	racemase and epimerase activity, acting on amino acids and derivatives	216524	4	0.91	0.64	
GO:0004022	endopeptidase inhibitor activity	216430	17	0.70	0.35	0.64 (0.43)
GO:0008409	alcohol dehydrogenase (NAD ⁺) activity	216214	0	0.93		
GO:0000149	5'-3' exonuclease activity	216117	0	0.90		
GO:001664	SNARE binding	212890	0	0.79		
GO:0004843	G protein-coupled receptor binding	212007	0	0.72		
GO:0008422	thiol-dependent ubiquitin-specific protease activity	211934	53	0.92	0.87	0.92 (0.86)
GO:0003727	beta-glucosidase activity	210397	12	0.87	0.62	0.89 (0.81)
GO:005539	single-stranded RNA binding	210015	2	0.74	0.49	
GO:0019904	glycosaminoglycan binding	209916	0	0.43		
GO:0004029	protein domain specific binding	206750	0	0.70		
GO:0005262	aldehyde dehydrogenase (NAD ⁺) activity	206208	11	0.93	0.71	0.96 (0.92)
GO:0016984	ribulose-bisphosphate carboxylase activity	205698	0	0.91		
GO:0050145	nucleoside monophosphate kinase activity	205183	24	0.73	0.54	0.67 (0.56)
GO:0042803	protein homodimerization activity	205135	0	0.82		
GO:0016880	acid-ammonia (or amide) ligase activity	204864	1	0.89		
GO:0099094	ligand-gated cation channel activity	204815	0	0.63		
GO:0005262	calcium channel activity	204609	0	0.68		
GO:0031177	phosphopantetheine binding	204490	0	0.85		
GO:0070567	cytidylyltransferase activity	200864	2	0.74	0.73	
GO:0034212	peptide N-acetyltransferase activity	199824	0	0.68		
GO:0008172	S-methyltransferase activity	198088	0	0.60		
GO:0003713	transcription coactivator activity	197855	0	0.74		
GO:0005254	chloride channel activity	197536	0	0.77		
GO:0016838	carbon-oxygen lyase activity, acting on phosphates	196873	0	0.95		
GO:0016837	carbon-oxygen lyase activity, acting on polysaccharides	196843	1	0.84		
GO:0047661	amino-acid racemase activity	196575	7	0.90	0.69	
GO:0004806	triglyceride lipase activity	196099	0	0.94		
GO:0008198	ferrous iron binding	195695	0	0.82		
GO:0016778	diphosphotransferase activity	195419	5	0.68	0.52	
GO:1901981	phosphatidylinositol phosphate binding	194666	0	0.74		
GO:0043178	alcohol binding	193651	0	0.82		
GO:0009008	DNA-methyltransferase activity	192797	10	0.84	0.64	
GO:0019208	phosphatase regulator activity	192040	0	0.91		
GO:0016151	nickel cation binding	188640	0	0.82		
GO:0004359	glutaminase activity	188116	5	0.88	0.79	
GO:0046527	glucosyltransferase activity	187437	6	0.89	0.71	
GO:0003725	double-stranded RNA binding	186664	0	0.77		
GO:0046812	host cell surface binding	186003	0	0.63		
GO:0046789	host cell surface receptor binding	185633	0	0.84		
GO:0004033	aldo-keto reductase (NADP) activity	184654	28	0.94	0.86	0.92 (0.79)
GO:0032182	ubiquitin-like protein binding	183324	0	0.78		
GO:0070181	small ribosomal subunit rRNA binding	181132	0	0.48		
GO:0016888	endo-deoxyribonuclease activity, producing 5'-phosphomonooesters	180109	4	0.94	0.81	
GO:0004364	glutathione transferase activity	180045	18	0.83	0.61	0.67 (0.56)
GO:0016722	oxidoreductase activity, oxidizing metal ions	179506	0	0.78		
GO:0043546	molybdopterin cofactor binding	178603	0	0.73		
GO:0019888	protein phosphatase regulator activity	178589	0	0.90		
GO:0008146	sulfotransferase activity	178506	3	0.91	0.82	
GO:0019202	amino acid kinase activity	178328	0	0.97		
GO:0005249	voltage-gated potassium channel activity	177385	0	0.65		
GO:0043023	ribosomal large subunit binding	174957	0	0.78		
GO:0016553	peptide receptor activity	174954	5	0.94	0.86	

Term	Description	Occurrences	Successes	scTM	TM-diversity	TM-novelty (min)
GO:0016813	hydrolase activity, acting on carbon-nitrogen (but not peptide) bonds, in linear...	174814	2	0.90	0.71	
GO:0003777	microtubule motor activity	173936	56	0.83	0.75	0.92 (0.53)
GO:0016417	S-acetyltransferase activity	172012	0	0.80		
GO:0016413	O-acetyltransferase activity	170516	2	0.86	0.79	
GO:0070402	NADPH binding	169977	1	0.97		
GO:0008134	transcription factor binding	168192	0	0.81		
GO:0008484	sulfuric ester hydrolase activity	168079	1	0.82		
GO:0043100	ubiquitin binding	167722	0	0.80		
GO:0070180	large ribosomal subunit rRNA binding	166128	7	0.59	0.28	
GO:0050897	cobalt ion binding	164184	0	0.80		
GO:0051119	sugar transmembrane transporter activity	164029	0	0.69		
GO:0019203	carbohydrate phosphatase activity	163095	0	0.93		
GO:0003906	DNA-(apurinic or apyrimidinic site) endonuclease activity	162862	0	0.87		
GO:0008252	nucleotidase activity	162804	0	0.92		
GO:0003988	acetyl-CoA C-acyltransferase activity	161603	38	0.86	0.76	0.91 (0.79)
GO:0003989	acetyl-CoA carboxylase activity	161496	6	0.77	0.66	
GO:0008982	protein-N(PI)-phosphohistidine-sugar phosphotransferase activity	161158	0	0.83		
GO:0008079	translation termination factor activity	160891	11	0.55	0.39	0.54 (0.38)
GO:0003747	translation release factor activity	160834	9	0.52	0.42	
GO:0070569	uridylyltransferase activity	160831	1	0.87		
GO:0030594	neurotransmitter receptor activity	160718	11	0.78	0.75	0.88 (0.81)
GO:0050308	sugar-phosphatase activity	160589	0	0.91		
GO:0005125	cytokine activity	159637	0	0.50		
GO:0016886	ligase activity, forming phosphoric ester bonds	159546	21	0.81	0.69	0.82 (0.76)
GO:0047134	protein-disulfide reductase activity	159034	0	0.83		
GO:0003730	mRNA 3'-UTR binding	157053	0	0.83		
GO:0016435	rRNA (guanine) methyltransferase activity	156873	2	0.76	0.61	
GO:0047617	acyl-CoA hydrolase activity	155267	0	0.92		
GO:0031072	heat shock protein binding	152679	28	0.62	0.40	0.58 (0.36)
GO:0016671	oxidoreductase activity, acting on a sulfur group of donors, disulfide as accept...	151809	0	0.64		
GO:0035251	UDP-glucosyltransferase activity	151466	1	0.90		
GO:0030151	molybdenum ion binding	151176	0	0.70		
GO:0015925	galactosidase activity	151121	0	0.86		
GO:0001882	nucleoside binding	149828	0	0.39		
GO:0016712	oxidoreductase activity, acting on paired donors, with incorporation or reductio...	149272	0	0.93		
GO:0016728	oxidoreductase activity, acting on CH or CH ₂ groups, disulfide as acceptor	149030	0	0.83		
GO:0032549	ribonucleoside binding	148548	1	0.38		
GO:0005548	phospholipid transporter activity	147516	0	0.71		
GO:0019199	transmembrane receptor protein kinase activity	147284	12	0.95	0.83	0.91 (0.89)
GO:0070063	RNA polymerase binding	146461	0	0.71		
GO:0001216	DNA-binding transcription activator activity	144929	0	0.69		
GO:0016842	amidine-lyase activity	144759	5	0.78	0.62	
GO:0009002	serine-type D-Ala-D-Ala carboxypeptidase activity	144645	0	0.84		
GO:0016805	dipeptidase activity	144534	0	0.88		
GO:0004748	ribonucleoside-diphosphate reductase activity, thioredoxin disulfide as acceptor	143802	0	0.83		
GO:00061731	ribonucleoside-diphosphate reductase activity	143802	0	0.83		
GO:0008199	ferric iron binding	143626	0	0.74		
GO:0016661	oxidoreductase activity, acting on other nitrogenous compounds as donors	142766	0	0.74		
GO:0008528	G protein-coupled peptide receptor activity	141652	0	0.94		
GO:0005200	structural constituent of cytoskeleton	141217	41	0.82	0.75	0.90 (0.75)
GO:0015145	monosaccharide transmembrane transporter activity	140757	20	0.92	0.69	0.88 (0.78)
GO:0044389	ubiquitin-like protein ligase binding	139168	0	0.75		
GO:0016615	malate dehydrogenase activity	138933	19	0.90	0.85	0.89 (0.78)
GO:0016278	lysine N-methyltransferase activity	138489	0	0.84		
GO:0016279	protein-lysine N-methyltransferase activity	138487	0	0.84		
GO:0070568	guanylyltransferase activity	137554	8	0.92	0.79	
GO:0004112	cyclic-nucleotide phosphodiesterase activity	137408	12	0.92	0.85	0.94 (0.87)
GO:0030551	cyclic nucleotide binding	136113	0	0.51		
GO:0016453	C-acetyltransferase activity	136095	15	0.86	0.82	0.91 (0.79)
GO:0004300	enoyl-CoA hydratase activity	136028	19	0.86	0.74	0.81 (0.69)
GO:0016168	chlorophyll binding	135298	0	0.41		
GO:0005230	extracellular ligand-gated ion channel activity	134950	23	0.81	0.79	0.90 (0.80)
GO:0016433	rRNA (adenine) methyltransferase activity	134300	0	0.83		
GO:0000150	recombinase activity	133802	0	0.66		
GO:0043024	ribosomal small subunit binding	133464	0	0.77		
GO:0008745	N-acetyl muramoyl-L-alanine amidase activity	132782	0	0.69		
GO:0004457	lactate dehydrogenase activity	132604	17	0.92	0.75	0.89 (0.61)
GO:0016641	oxidoreductase activity, acting on the CH-NH ₂ group of donors, oxygen as accepto...	132222	0	0.53		
GO:0042054	histone methyltransferase activity	131874	67	0.60	0.54	0.65 (0.54)
GO:00060590	ATPase regulator activity	131859	0	0.75		
GO:0003796	lysozyme activity	131568	1	0.70		
GO:0016882	cyclo-ligase activity	131477	0	0.85		
GO:0004867	serine-type endopeptidase inhibitor activity	131355	21	0.68	0.31	0.54 (0.43)
GO:0004596	peptide alpha-N-acetyltransferase activity	130998	0	0.63		
GO:0003909	DNA ligase activity	130798	16	0.79	0.66	0.81 (0.72)
GO:0005126	cytokine receptor binding	130687	0	0.53		
GO:0004549	tRNA-specific ribonuclease activity	130472	0	0.88		
GO:0004550	nucleoside diphosphate kinase activity	129618	54	0.59	0.52	0.66 (0.52)
GO:0004396	hexokinase activity	129154	5	0.91	0.65	
GO:0008379	thioredoxin peroxidase activity	128653	1	0.65		
GO:0004040	amidase activity	128580	0	0.66		
GO:0008083	growth factor activity	128255	0	0.54		
GO:0031625	ubiquitin protein ligase binding	127226	0	0.68		
GO:0016211	ammonia ligase activity	127146	0	0.88		
GO:0004792	thiosulfate sulfurtransferase activity	126733	3	0.90	0.61	
GO:0019209	kinase activator activity	126228	0	0.94		
GO:0016423	tRNA (guanine) methyltransferase activity	126219	0	0.77		
GO:0030295	protein kinase activator activity	125086	0	0.89		
GO:0050497	transfase activity, transferring alkylthio groups	124481	46	0.89	0.62	0.82 (0.52)
GO:0008641	ubiquitin-like modifier activating enzyme activity	124419	77	0.82	0.71	0.79 (0.68)

Term	Description	Occurrences	Successes	scTM	TM-diversity	TM-novelty (min)
GO:0016997	alpha-sialidase activity	123365	0	0.93		
GO:0017116	single-stranded DNA helicase activity	123289	0	0.81		
GO:0004308	exo-alpha-sialidase activity	123268	0	0.89		
GO:0070492	oligosaccharide binding	122506	0	0.90		
GO:0008296	3'-5'-exodeoxyribonuclease activity	122442	0	0.89		
GO:0016634	oxidoreductase activity, acting on the CH-CH group of donors, oxygen as acceptor	122047	0	0.73		
GO:0005496	steroid binding	121906	0	0.62		
GO:0030247	polysaccharide binding	121859	0	0.56		
GO:0070003	threonine-type peptidase activity	121768	4	0.67	0.53	
GO:0016208	AMP binding	120190	0	0.81		
GO:0051117	ATPase binding	119932	0	0.67		
GO:0004791	thioredoxin-disulfide reductase activity	119540	1	0.76		
GO:0008061	chitin binding	119224	31	0.59	0.65	0.87 (0.68)
GO:0008106	alcohol dehydrogenase (NADP+) activity	119030	14	0.95	0.87	0.92 (0.82)
GO:0008410	CoA-transferase activity	118984	0	0.79		
GO:0008395	steroid hydroxylase activity	118669	0	0.93		
GO:0008253	5'-nucleotidase activity	118026	0	0.91		
GO:0032451	demethylase activity	117409	0	0.84		
GO:1902936	phosphatidylinositol bisphosphate binding	116902	0	0.85		
GO:0004714	transmembrane receptor protein tyrosine kinase activity	115999	0	0.93		
GO:0015923	mannosidase activity	115861	0	0.79		
GO:0016682	oxidoreductase activity, acting on diphenols and related substances as donors, o...	115149	0	0.65		
GO:0016229	steroid dehydrogenase activity	114186	0	0.91		
GO:0016639	oxidoreductase activity, acting on the CH-NH ₂ group of donors, NAD or NADP as ac...	113639	7	0.86	0.58	
GO:0015450	P-P bond-hydrolysis-driven protein transmembrane transporter activity	113279	83	0.69	0.60	0.70 (0.48)
GO:0003688	DNA replication origin binding	113128	0	0.82		
GO:0045156	electron transporter, transferring electrons within the cyclic electron transpor...	112773	0	0.42		
GO:0045296	cadherin binding	112694	0	0.73		
GO:0019210	kinase inhibitor activity	111643	0	0.75		
GO:0051538	3 iron, 4 sulfur cluster binding	111245	2	0.74	0.37	
GO:0004312	fatty acid synthase activity	111193	18	0.82	0.64	0.89 (0.75)
GO:0008443	phosphofructokinase activity	110770	28	0.86	0.73	0.87 (0.79)
GO:0004860	protein kinase inhibitor activity	109362	0	0.72		
GO:0016247	channel regulator activity	109309	0	0.88		
GO:0042562	hormone binding	109244	0	0.66		
GO:0004000	adenosine deaminase activity	109130	0	0.97		
GO:0031420	alkali metal ion binding	107342	0	0.76		
GO:0016538	cyclin-dependent protein serine/threonine kinase regulator activity	107306	2	0.84	0.77	
GO:0004764	shikimate 3-dehydrogenase (NADP+) activity	107144	2	0.94	0.80	
GO:0004731	purine-nucleoside phosphorylase activity	106641	2	0.91	0.76	
GO:0031490	chromatin DNA binding	106252	0	0.82		
GO:0098960	postsynaptic neurotransmitter receptor activity	106177	5	0.77	0.79	
GO:0016863	intramolecular oxidoreductase activity, transposing C=C bonds	105994	0	0.85		
GO:0048030	disaccharide binding	105877	0	0.90		
GO:0004181	metallocarboxypeptidase activity	105742	2	0.93	0.86	
GO:0008242	omega peptidase activity	105199	0	0.66		
GO:0022824	transmitter-gated ion channel activity	105050	4	0.77	0.80	
GO:0022835	transmitter-gated channel activity	105050	6	0.76	0.75	
GO:0008239	dipeptidyl-peptidase activity	104787	0	0.78		
GO:0032934	sterol binding	103880	0	0.61		
GO:0099106	ion channel regulator activity	103681	0	0.88		
GO:0140223	general transcription initiation factor activity	103467	0	0.87		
GO:0009041	uridylylate kinase activity	103186	0	0.84		
GO:0008840	4-hydroxy-tetrahydridopicolinate synthase activity	101408	1	0.93		
GO:0003823	antigen binding	101339	0	0.67		
GO:0140375	immune receptor activity	101229	1	0.52		
GO:0106130	purine phosphoribosyltransferase activity	101220	38	0.61	0.51	0.53 (0.45)
GO:1904047	S-adenosyl-L-methionine binding	100025	11	0.91	0.67	0.75 (0.63)
GO:0052745	inositol phosphate phosphatase activity	99479	50	0.95	0.79	0.83 (0.76)
GO:0005549	odorant binding	99450	0	0.84		
GO:0030276	clathrin binding	99167	0	0.87		
GO:0090729	toxin activity	99166	1	0.79		
GO:0050136	NADH dehydrogenase (quinone) activity	98827	0	0.81		
GO:0003855	3-dehydroquinate dehydratase activity	96857	0	0.84		
GO:0016822	hydrolase activity, acting on acid carbon-carbon bonds	96299	0	0.73		
GO:0016823	hydrolase activity, acting on acid carbon-carbon bonds, in ketonic substances	96297	0	0.75		
GO:0005504	fatty acid binding	96242	0	0.77		
GO:0030291	protein serine/threonine kinase inhibitor activity	95388	0	0.67		
GO:0004322	ferroxidase activity	95039	0	0.83		
GO:0016724	oxidoreductase activity, oxidizing metal ions, oxygen as acceptor	95039	0	0.82		
GO:0008097	5S rRNA binding	94984	0	0.48		
GO:0140297	DNA-binding transcription factor binding	94976	0	0.92		
GO:0098531	ligand-activated transcription factor activity	94954	1	0.77		
GO:0004879	nuclear receptor activity	94890	2	0.79	0.68	
GO:0043891	glyceraldehyde-3-phosphate dehydrogenase (NAD(P)+) (phosphorylating) activity	94775	33	0.89	0.80	0.90 (0.85)
GO:0004834	tryptophan synthase activity	94526	1	0.93		
GO:0009881	photoreceptor activity	94518	1	0.95		
GO:0004365	glyceraldehyde-3-phosphate dehydrogenase (NAD+) (phosphorylating) activity	94301	28	0.90	0.81	0.90 (0.85)
GO:0030955	potassium ion binding	93971	0	0.76		
GO:1901982	maltose binding	92877	0	0.90		
GO:0031491	nucleosome binding	92324	0	0.94		
GO:0000104	succinate dehydrogenase activity	92085	0	0.70		
GO:0016748	succinyltransferase activity	91428	0	0.85		
GO:0004089	carbonate dehydratase activity	91332	1	0.73		
GO:0140034	methylation-dependent protein binding	90791	0	0.73		
GO:0019212	phosphatase inhibitor activity	90433	0	0.52		
GO:0004896	cytokine receptor activity	90357	0	0.53		
GO:0042834	peptidoglycan binding	90349	0	0.42		
GO:0016801	hydrolase activity, acting on ether bonds	90047	0	0.94		
GO:0035064	methylated histone binding	89875	0	0.70		

Term	Description	Occurrences	Successes	scTM	TM-diversity	TM-novelty (min)
GO:0016803	ether hydrolase activity	89708	0	0.95		
GO:0005179	hormone activity	89038	0	0.58		
GO:0120013	lipid transfer activity	89032	0	0.80		
GO:0005178	integrin binding	88855	0	0.73		
GO:0016251	RNA polymerase II general transcription initiation factor activity	88449	0	0.88		
GO:0019825	oxygen binding	88439	11	0.67	0.54	0.66 (0.54)
GO:0004565	beta-galactosidase activity	88416	0	0.81		
GO:0035438	cyclic-di-GMP binding	88299	0	0.51		
GO:0004590	rotidinone-5'-phosphate decarboxylase activity	87823	0	0.92		
GO:0003955	NAD(P)H dehydrogenase (quinone) activity	87744	0	0.86		
GO:0016635	oxidoreductase activity, acting on the CH-CH group of donors, quinone or related...	86780	0	0.66		
GO:0019905	syntaxin binding	86767	0	0.83		
GO:0016730	oxidoreductase activity, acting on iron-sulfur proteins as donors	86672	0	0.81		
GO:0004124	cysteine synthase activity	85914	8	0.94	0.89	
GO:0004427	inorganic diphosphatase activity	84917	0	0.65		
GO:0003993	acid phosphatase activity	84881	1	0.88		
GO:0004017	adenylate kinase activity	84862	21	0.78	0.61	0.68 (0.62)
GO:0004864	protein phosphatase inhibitor activity	84732	0	0.49		
GO:0016160	amylase activity	84411	1	0.91		
GO:0004148	dihydrolipoyl dehydrogenase activity	84293	0	0.86		
GO:0005544	calcium-dependent phospholipid binding	84017	1	0.81		
GO:0106310	protein serine kinase activity	83197	0	0.92		
GO:0015929	hexosaminidase activity	83067	0	0.86		
GO:0004568	chitinase activity	82641	13	0.90	0.81	0.92 (0.87)
GO:0099529	neurotransmitter receptor activity involved in regulation of postsynaptic membra...	82302	0	0.78		
GO:1904315	transmitter-gated ion channel activity involved in regulation of postsynaptic me...	82225	2	0.78	0.85	
GO:0019955	cytokine binding	81949	0	0.53		
GO:0004045	aminoacyl-tRNA hydrolase activity	81568	2	0.66	0.56	
GO:0097506	deaminated base DNA N-glycosylase activity	81342	0	0.78		
GO:0004844	uracil DNA N-glycosylase activity	81340	0	0.78		
GO:0016426	tRNA (adenine) methyltransferase activity	81261	0	0.43		
GO:0004448	isocitrate dehydrogenase activity	80443	0	0.83		
GO:0120227	acyl-CoA binding	79466	0	0.84		
GO:0004556	alpha-amylase activity	78847	0	0.90		
GO:0016703	oxidoreductase activity, acting on single donors with incorporation of molecular...	78560	0	0.82		
GO:0019206	nucleoside kinase activity	78259	1	0.85		
GO:0001217	DNA-binding transcription repressor activity	78251	0	0.73		
GO:0140142	nucleocytoplasmic carrier activity	78120	0	0.94		
GO:0140078	class I DNA-(apurinic or apyrimidinic site) endonuclease activity	77966	0	0.83		
GO:0004645	1,4-alpha-oligoglucan phosphorylase activity	77815	0	0.87		
GO:0030515	snRNA binding	77321	0	0.85		
GO:0004114	3',5'-cyclic-nucleotide phosphodiesterase activity	77176	12	0.92	0.88	0.95 (0.93)
GO:0016721	oxidoreductase activity, acting on superoxide radicals as acceptor	76863	4	0.66	0.52	
GO:0033764	steroid dehydrogenase activity, acting on the CH-OH group of donors, NAD or NADP..	76840	0	0.94		
GO:1901567	fatty acid derivative binding	76815	0	0.89		
GO:0000062	fatty-acyl-CoA binding	76785	0	0.85		
GO:0004640	phosphoribosylanthranilate isomerase activity	76311	0	0.75		
GO:0019902	phosphatase binding	75964	0	0.88		
GO:0032296	double-stranded RNA-specific ribonuclease activity	75608	4	0.70	0.51	
GO:0004525	ribonuclease III activity	75603	3	0.70	0.60	
GO:0042162	telomeric DNA binding	75557	0	0.73		
GO:0043175	RNA polymerase core enzyme binding	75471	0	0.76		
GO:0061733	peptide-lysine-N-acetyltransferase activity	75073	0	0.78		
GO:0008201	heparin binding	75051	0	0.56		
GO:0017056	structural constituent of nuclear pore	74472	0	0.79		
GO:0004459	L-lactate dehydrogenase activity	74414	38	0.95	0.89	0.94 (0.86)
GO:0005546	phosphatidylinositol-4,5-bisphosphate binding	74214	0	0.81		
GO:0004623	phospholipase A2 activity	74203	0	0.68		
GO:0004784	superoxide dismutase activity	74175	3	0.69	0.58	
GO:0008800	beta-lactamase activity	74086	0	0.85		
GO:0019838	growth factor binding	73901	0	0.90		
GO:0008897	holo-[acyl-carrier-protein] synthase activity	73451	0	0.86		
GO:0015038	glutathione disulfide oxidoreductase activity	73388	0	0.63		
GO:0140414	phosphopantetheine-dependent carrier activity	72951	1	0.74		
GO:0004106	chorismate mutase activity	72673	0	0.48		
GO:0004332	fructose-bisphosphate aldolase activity	72616	0	0.96		
GO:0004831	tyrosine-tRNA ligase activity	72406	28	0.92	0.75	0.84 (0.77)
GO:0051192	prosthetic group binding	72138	1	0.74		
GO:0044620	ACP phosphopantetheine attachment site binding	72127	0	0.78		
GO:0000036	acyl carrier activity	72127	0	0.80		
GO:0008312	7S RNA binding	71012	0	0.77		
GO:0004096	catalase activity	70609	0	0.36		
GO:004325	ion channel binding	70512	0	0.89		
GO:0015485	cholesterol binding	69630	0	0.62		
GO:0070401	NADP+ binding	69023	0	0.94		
GO:0004402	histone acetyltransferase activity	68538	0	0.84		
GO:0005324	long-chain fatty acid transporter activity	68175	0	0.80		
GO:0035591	signaling adaptor activity	68129	0	0.85		
GO:0004634	phosphopyruvate hydratase activity	68112	1	0.85		
GO:0005245	voltage-gated calcium channel activity	67966	0	0.64		
GO:0017069	snRNA binding	67622	0	0.91		
GO:0004526	ribonuclease P activity	66470	3	0.56	0.36	
GO:0042586	peptide deformylase activity	66451	1	0.65		
GO:0004347	glucose-6-phosphate isomerase activity	66366	3	0.81	0.70	
GO:0036402	proteasome-activating ATPase activity	66266	2	0.81	0.69	
GO:0004619	phosphoglycerate mutase activity	66265	0	0.78		
GO:0004372	glycine hydroxymethyltransferase activity	66253	0	0.83		
GO:0070851	growth factor receptor binding	66113	0	0.58		
GO:0001098	basal transcription machinery binding	66048	0	0.73		
GO:0001099	basal RNA polymerase II transcription machinery binding	66042	0	0.77		

Term	Description	Occurrences	Successes	scTM	TM-diversity	TM-novelty (min)
GO:0000179	rRNA (adenine-N6,N6')-dimethyltransferase activity	65590	1	0.90		
GO:0015666	restriction endodeoxyribonuclease activity	65512	0	0.73		
GO:0008716	D-alanine-D-alanine ligase activity	65500	0	0.96		
GO:0003910	DNA ligase (ATP) activity	65271	1	0.79		
GO:0006129	RNA polymerase II-specific DNA-binding transcription factor binding	65095	0	0.91		
GO:0031418	L-ascorbic acid binding	64743	0	0.79		
GO:0004316	3-oxoacyl-[acyl-carrier-protein] reductase (NADPH) activity	63867	35	0.89	0.81	0.83 (0.74)
GO:0014296	general transcription initiation factor binding	63469	4	0.65	0.42	
GO:0004563	beta-N-acetylhexosaminidase activity	62880	0	0.91		
GO:0008477	purine nucleosidase activity	62159	0	0.93		
GO:0004715	non-membrane spanning protein tyrosine kinase activity	62155	0	0.88		
GO:0017022	myosin binding	62079	0	0.66		
GO:0004807	triose-phosphate isomerase activity	61975	1	0.89		
GO:0005231	excitatory extracellular ligand-gated ion channel activity	61781	2	0.78	0.73	
GO:0016889	endodeoxyribonuclease activity, producing 3'-phosphomonooesters	61638	0	0.73		
GO:0019903	protein phosphatase binding	61183	0	0.91		
GO:0003857	3-hydroxyacyl-CoA dehydrogenase activity	61127	4	0.87	0.76	
GO:0003938	IMP dehydrogenase activity	60808	0	0.63		
GO:0008948	oxaloacetate decarboxylase activity	60562	0	0.74		
GO:0042083	5,10-methylenetetrahydrolipoyl-dependent methyltransferase activity	60447	0	0.81		
GO:0004830	tryptophan-tRNA ligase activity	60297	2	0.93	0.82	
GO:0043539	protein serine/threonine kinase activator activity	59633	0	0.92		
GO:0008174	mRNA methyltransferase activity	59365	4	0.87	0.61	
GO:0045182	translation regulator activity	59127	0	0.79		
GO:0005344	oxygen carrier activity	58966	11	0.67	0.53	0.64 (0.59)
GO:0004799	thymidylate synthase activity	58788	0	0.80		
GO:0008066	glutamate receptor activity	57432	0	0.74		
GO:0004450	isocitrate dehydrogenase (NADP+) activity	57116	0	0.75		
GO:0003950	NAD+ ADP-ribosyltransferase activity	56999	0	0.70		
GO:0016273	arginine N-methyltransferase activity	56907	9	0.85	0.81	
GO:0016274	protein-arginine N-methyltransferase activity	56907	5	0.86	0.77	
GO:0004422	hypoxanthine phosphoribosyltransferase activity	56847	11	0.57	0.53	0.56 (0.52)
GO:0004618	phosphoglycerate kinase activity	56455	0	0.76		
GO:0004602	glutathione peroxidase activity	56445	0	0.69		
GO:0006150	ubiquitin-like protein conjugating enzyme activity	56308	36	0.66	0.52	0.59 (0.51)
GO:0004557	alpha-galactosidase activity	55838	0	0.91		
GO:0000993	RNA polymerase II complex binding	55653	0	0.76		
GO:0031369	translation initiation factor binding	55632	0	0.83		
GO:0022839	ion gated channel activity	55300	0	0.65		
GO:0016726	oxidoreductase activity, acting on CH or CH ₂ groups, NAD or NADP as acceptor	55254	0	0.75		
GO:0003952	NAD+ synthase (glutamine-hydrolyzing) activity	54234	12	0.77	0.63	0.68 (0.57)
GO:0036002	pre-mRNA binding	53968	0	0.52		
GO:0004585	ornithine carbamoyltransferase activity	53952	0	0.93		
GO:0030060	L-lactate dehydrogenase activity	53907	50	0.91	0.87	0.91 (0.81)
GO:0008784	alanine racemase activity	53689	0	0.76		
GO:0004751	ribose-5-phosphate isomerase activity	53270	2	0.68	0.51	
GO:0004712	protein serine/threonine/tyrosine kinase activity	52858	0	0.94		
GO:0016670	oxidoreductase activity, acting on a sulfur group of donors, oxygen as acceptor	52569	0	0.48		
GO:0004298	threonine-type endopeptidase activity	52158	19	0.70	0.64	0.70 (0.63)
GO:0042132	fructose 1,6-bisphosphate 1-phosphatase activity	52113	17	0.95	0.79	0.81 (0.76)
GO:0004629	phospholipase C activity	52108	0	0.70		
GO:0016420	malonyltransferase activity	51857	50	0.94	0.89	0.93 (0.83)
GO:0016419	S-malonyltransferase activity	51809	54	0.94	0.88	0.93 (0.82)
GO:0004314	[acyl-carrier-protein] S-malonyltransferase activity	51809	48	0.92	0.89	0.93 (0.86)
GO:0008227	G protein-coupled amine receptor activity	50580	0	0.94		
GO:0016872	intramolecular lyase activity	50575	0	0.63		
GO:0042301	phosphate ion binding	50483	0	0.86		
GO:0046556	alpha-L-arabinofuranosidase activity	50450	0	0.89		
GO:0004156	dihydropteroate synthase activity	49975	2	0.95	0.72	
GO:0008839	4-hydroxy-tetrahydridopicolinate reductase	49189	7	0.95	0.73	
GO:00061631	ubiquitin conjugating enzyme activity	48787	39	0.62	0.52	0.58 (0.51)
GO:00061608	nuclear import signal receptor activity	48698	0	0.96		
GO:0015616	DNA translocase activity	48403	0	0.87		
GO:0017025	TBP-class protein binding	47270	3	0.70	0.38	
GO:0008810	cellulase activity	46628	0	0.75		
GO:0005227	calcium activated cation channel activity	46100	0	0.67		
GO:0016631	enoyl-[acyl-carrier-protein] reductase activity	46043	0	0.91		
GO:0004340	glucokinase activity	46028	5	0.89	0.81	
GO:0000339	RNA cap binding	45753	0	0.84		
GO:0004146	dihydrofolate reductase activity	45388	1	0.70		
GO:0016731	oxidoreductase activity, acting on iron-sulfur proteins as donors, NAD or NADP a...	44648	0	0.89		
GO:0097599	xylanase activity	44080	0	0.87		
GO:0016695	oxidoreductase activity, acting on hydrogen as donor	43949	2	0.41	0.29	
GO:0005217	intracellular ligand-gated ion channel activity	43879	0	0.70		
GO:1990782	protein tyrosine kinase binding	43531	0	0.58		
GO:0004318	enoyl-[acyl-carrier-protein] reductase (NADH) activity	43314	0	0.91		
GO:0008795	NAD+ synthase activity	43133	4	0.81	0.61	
GO:0004170	dUTP diphosphatase activity	42889	14	0.43	0.59	0.69 (0.43)
GO:0038024	cargo receptor activity	42267	0	0.41		
GO:0008937	ferredoxin-NAD(P) reductase activity	42025	0	0.91		
GO:0004425	indole-3-glycerol-phosphate synthase activity	41761	1	0.78		
GO:0032813	tumor necrosis factor receptor superfamily binding	41738	0	0.50		
GO:0033818	beta-ketoacyl-acyl-carrier-protein synthase III activity	41686	10	0.96	0.83	
GO:0004514	nicotinate-nucleotide diphosphorylase (carboxylating) activity	41609	0	0.91		
GO:0001671	ATPase activator activity	41553	0	0.53		
GO:0004707	MAP kinase activity	41257	9	0.93	0.80	
GO:0051018	protein kinase A binding	40484	0	0.60		
GO:0004324	ferredoxin-NADP+ reductase activity	40483	0	0.92		
GO:0051219	phosphoprotein binding	39966	0	0.86		
GO:0003756	protein disulfide isomerase activity	39963	47	0.55	0.46	0.63 (0.51)

Term	Description	Occurrences	Successes	scTM	TM-diversity	TM-novelty (min)
GO:0016864	intramolecular oxidoreductase activity, transposing S-S bonds	39963	54	0.53	0.46	0.62 (0.54)
GO:0016699	oxidoreductase activity, acting on hydrogen as donor, iron-sulfur protein as acceptor	39010	0	0.44		
GO:0008901	ferredoxin hydrogenase activity	39010	0	0.45		
GO:0004567	beta-mannosidase activity	38746	0	0.85		
GO:0004482	mRNA (guanine-N7-)methyltransferase activity	38510	2	0.84	0.46	
GO:0045309	protein phosphorylated amino acid binding	38374	0	0.64		
GO:0004069	L-aspartate:2-oxoglutarate aminotransferase activity	37777	0	0.77		
GO:0030971	receptor tyrosine kinase binding	37465	0	0.58		
GO:0001046	core promoter sequence-specific DNA binding	37260	0	0.67		
GO:0005536	glucose binding	37050	6	0.88	0.79	
GO:0031386	protein tag	36824	14	0.39	0.51	0.72 (0.54)
GO:0019003	GDP binding	36588	0	0.66		
GO:0019840	isoprenoid binding	36505	0	0.74		
GO:0004126	cytidine deaminase activity	36462	2	0.54	0.49	
GO:0031683	G-protein beta/gamma-subunit complex binding	36293	11	0.87	0.79	0.88 (0.82)
GO:0008138	protein tyrosine/serine/threonine phosphatase activity	36282	61	0.67	0.52	0.61 (0.55)
GO:0051879	Hsp90 protein binding	35773	0	0.89		
GO:0016917	GABA receptor activity	34681	0	0.84		
GO:0099604	ligand-gated calcium channel activity	34359	0	0.68		
GO:0016899	oxidoreductase activity, acting on the CH-OH group of donors, oxygen as acceptor	33613	0	0.89		
GO:0042800	histone methyltransferase activity (H3-K4 specific)	33562	0	0.58		
GO:0004970	ionotropic glutamate receptor activity	33271	0	0.67		
GO:0008013	beta-catenin binding	33221	0	0.67		
GO:0009678	pyrophosphate hydrolysis-driven proton transmembrane transporter activity	33198	0	0.74		
GO:0016504	peptidase activator activity	32834	0	0.90		
GO:0004032	aliditol:NADP+ 1-oxidoreductase activity	32729	14	0.92	0.89	0.94 (0.91)
GO:0016892	endoribonuclease activity, producing 3'-phosphomonooesters	31944	0	0.57		
GO:0004551	nucleotide diphosphatase activity	31619	7	0.64	0.54	
GO:0016662	oxidoreductase activity, acting on other nitrogenous compounds as donors, cytochrome	30872	0	0.66		
GO:0042826	histone deacetylase binding	30860	0	0.78		
GO:0010333	terpene synthase activity	30523	4	0.87	0.71	
GO:0016843	amine-lyase activity	30019	0	0.86		
GO:0042379	chemokine receptor binding	29781	0	0.34		
GO:0002020	protease binding	29693	0	0.82		
GO:0050840	extracellular matrix binding	28977	0	0.49		
GO:0004675	transmembrane receptor protein serine/threonine kinase activity	28792	7	0.93	0.81	
GO:0004869	cysteine-type endopeptidase inhibitor activity	28718	0	0.47		
GO:0052657	guanine phosphoribosyltransferase activity	28595	7	0.56	0.50	
GO:0008930	methylthioadenosine nucleosidase activity	28292	0	0.85		
GO:0008782	adenosylhomocysteine nucleosidase activity	27918	0	0.89		
GO:0001530	lipopolysaccharide binding	27747	0	0.63		
GO:0005044	scavenger receptor activity	27168	0	0.39		
GO:0030248	cellulose binding	26936	0	0.61		
GO:0048027	mRNA 5'-UTR binding	26521	0	0.49		
GO:0005518	collagen binding	25946	0	0.64		
GO:0004362	glutathione-disulfide reductase activity	25845	0	0.86		
GO:0015278	calcium-release channel activity	25745	0	0.68		
GO:2001070	starch binding	25373	0	0.67		
GO:0005212	structural constituent of eye lens	24863	0	0.45		
GO:0034511	U3 snrRNA binding	24693	0	0.81		
GO:0008009	chemokine activity	24518	0	0.37		
GO:0098809	nitrite reductase activity	24508	0	0.78		
GO:0051427	hormone receptor binding	24420	0	0.74		
GO:0031176	endo-1,4-beta-xylanase activity	24420	0	0.80		
GO:0016248	channel inhibitor activity	24377	0	0.69		
GO:0008200	ion channel inhibitor activity	24320	0	0.76		
GO:0017080	sodium channel regulator activity	23696	0	0.72		
GO:0017154	semaphorin receptor activity	23677	0	0.67		
GO:0005024	coenzyme-B sulfoethylthiotransferase activity	23651	0	0.62		
GO:0016985	mannan endo-1,4-beta-mannosidase activity	23160	0	0.92		
GO:0016824	hydrolase activity, acting on acid halide bonds	22939	0	0.88		
GO:0019120	hydrolase activity, acting on acid halide bonds, in C-halide compounds	22930	0	0.89		
GO:0005164	tumor necrosis factor receptor binding	22834	0	0.49		
GO:0016708	oxidoreductase activity, acting on paired donors, with incorporation or reductio...	22266	0	0.88		
GO:0004483	mRNA (nucleoside-2'-O-)methyltransferase activity	21306	0	0.84		
GO:0005501	retinoid binding	21122	0	0.79		
GO:0005246	calcium channel regulator activity	20540	0	0.74		
GO:0003785	actin monomer binding	20314	0	0.51		
GO:0001540	amyloid-beta binding	20232	0	0.69		
GO:0048306	calcium-dependent protein binding	19589	0	0.55		
GO:0002039	p53 binding	19438	0	0.85		
GO:0005104	fibroblast growth factor receptor binding	18920	0	0.54		
GO:0034618	arginine binding	18834	0	0.64		
GO:0016972	thiol oxidase activity	17606	0	0.60		
GO:0035254	glutamate receptor binding	17506	0	0.80		
GO:0045735	nutrient reservoir activity	16951	2	0.81	0.66	
GO:1900750	oligopeptide binding	15092	0	0.88		
GO:0043295	glutathione binding	15045	0	0.89		
GO:0048487	beta-tubulin binding	14904	0	0.79		
GO:0009036	type II site-specific deoxyribonuclease activity	14686	0	0.86		
GO:0010427	abscisic acid binding	14290	0	0.67		
GO:0005537	mannose binding	13983	0	0.72		
GO:0015026	coreceptor activity	12746	0	0.35		
GO:0097718	disordered domain specific binding	12588	0	0.60		
GO:0030337	DNA polymerase processivity factor activity	11448	0	0.85		
GO:0050421	nitrite reductase (NO-forming) activity	11402	3	0.82	0.72	
GO:0015643	toxic substance binding	10829	0	0.85		
GO:0031720	haptoglobin binding	10250	0	0.67		
GO:0052716	hydroquinone:oxygen oxidoreductase activity	9876	0	0.77		
GO:0019871	sodium channel inhibitor activity	8600	0	0.63		

Term	Description	Occurrences	Successes	scTM	TM-diversity	TM-novelty (min)
GO:0008135	translation factor activity, RNA binding	8319	1	0.52		
GO:0080030	methyl indole-3-acetate esterase activity	7849	0	0.95		
GO:0034987	immunoglobulin receptor binding	5373	0	0.64		
GO:0048020	CCR chemokine receptor binding	4975	0	0.46		
GO:0019865	immunoglobulin binding	4897	0	0.87		
GO:0030597	RNA glycosylase activity	3696	0	0.40		
GO:0030598	rRNA N-glycosylase activity	3633	0	0.50		
GO:0009374	biotin binding	3138	0	0.61		
GO:0016018	cyclosporin A binding	2759	19	0.63	0.53	0.61 (0.55)
GO:0032052	bile acid binding	2328	0	0.91		
GO:0070404	NADH binding	2238	0	0.93		
GO:0016918	retinal binding	2113	0	0.60		
GO:0016894	endonuclease activity, active with either ribo- or deoxyribonucleic acids and pr...	1605	0	0.66		
GO:0001883	purine nucleoside binding	848	0	0.90		
GO:0005527	macrolide binding	264	0	0.86		
GO:1903981	enterobactin binding	106	0	0.86		
GO:0032550	purine ribonucleoside binding	4	0	0.88		

Table S2: Additional results on active site structural alignments. For each of 45 GO terms, we randomly select up to 5 successful designs and, for each design, highlight one of the aligned AFDB / UniProt structures. We report the all-atom active site RMSD, the % of matching residue identities within 5 Å of the active site, the overall sequence identity, and the active site residues annotated in UniProtKB.

Term	Sample	AFDB / UniProt ID	Active site RMSD	5 Å ID	Seq. ID	Active site residues
GO:0003988	1	P07871	0.05	66.67	48.67	C123,C408
	2	Q7A2W9	0.16	63.64	43.0	C86,H338
GO:0004029	1	A0A3Q7PKI4	0.13	80.95	45.33	E210,C244
	2	A0A1L7TDK2	0.16	70.59	42.0	E228,C262
	3	A0A7W3NA22	0.2	90.48	54.33	E254,C288
	4	A0A2S5TF45	0.18	61.11	46.67	E221,C255
	5	A0A7X3WQ03	0.23	52.63	44.67	E214,C248
GO:0004030	1	A0A2D9E9P2	0.17	64.71	43.0	E190,C224
	2	P52476	0.28	68.75	46.67	E279,C313
	3	A6UQD0	0.24	66.67	42.33	E240,C274
	4	B8M9E2	0.41	61.11	39.0	E228,C262
	5	A0A7V9U005	0.15	72.22	57.33	E260,C294
GO:0004032	1	O13848	0.28	57.14	39.44	Y54,H109
	2	Q07551	0.13	45.0	41.67	Y64,H122
	3	Q07551	0.25	54.17	36.0	Y64,H122
	4	O13848	0.21	61.9	40.49	Y54,H109
	5	O14088	0.22	52.17	36.73	Y50,H111
GO:0004033	1	O14088	0.17	41.67	36.36	Y50,H111
	2	O14088	0.16	54.55	39.64	Y50,H111
	3	O13848	0.37	56.52	41.2	Y54,H109
	4	Q76L36	0.42	60.87	41.67	Y63,H125
	5	O14088	0.31	41.67	40.36	Y50,H111
GO:0004177	1	A0A0Q4DGT6	0.49	66.67	51.67	K256,R330
GO:0004190	1	A0A6P7MYT9	0.25	40.91	38.0	I139,T325
	2	A0A1L9WSA4	0.29	66.67	43.67	D82,D279
	3	A0A0D9RBZ8	0.29	72.22	45.0	D97,D295
	4	A0A319CTT4	0.19	66.67	35.33	D50,D252
	5	B8YJG5	0.16	65.22	38.0	D108,D291
GO:0004197	1	Q9GL24	0.11	81.82	46.33	C138,H277,N300
	2	Q10991	0.17	85.29	51.61	C25,H163,N184
	3	P09648	0.17	70.59	49.08	C25,H165,N185
GO:0004252	1	U9V2T3	0.15	58.62	39.06	D18,H50,S209
	2	A0A7V7QN85	0.16	66.67	38.0	D29,H61,S244
	3	A0A1I6AYN1	0.27	75.0	50.67	D178,H217,S434
	4	A0A1I5DDV9	0.15	77.42	49.33	D62,H110,S292
	5	A0A7X2J0A2	0.17	79.41	44.33	D137,H174,S352
GO:0004312	1	A0A6L7X5E9	0.22	54.17	41.33	S128,H233
	2	A0A535J0M4	0.46	45.83	39.0	S103,H212
	3	A0A3M1LXU7	0.48	47.83	39.33	S94,H201
	4	A0A2E6YIR2	0.3	60.0	37.0	S103,H208
	5	A0A2M8ETE7	0.2	42.86	33.0	S114,H219
GO:0004314	1	A0A352PU99	0.31	26.92	35.33	S91,H196
	2	A0A496AKM2	0.2	57.69	38.67	S96,H204
	3	A0A2J0KPU7	0.18	53.85	38.0	S145,H250
	4	Q5F4X7	0.2	53.85	37.0	S90,H199
	5	A0A1G3UH18	0.21	65.38	31.33	S92,H202
GO:0004315	1	P9WQD9	0.63	37.93	44.67	C171,H311,H345
	2	P0AAI7	0.24	56.67	43.0	C164,H304,H341

Term	Sample	AFDB / UniProt ID	Active site RMSD	5 Å ID	Seq. ID	Active site residues
GO:0004525	1	A0A0F2Q590	0.14	56.52	30.29	D54,E126
	2	A0A535S225	0.05	56.52	34.91	D54,E124
	3	A0A2D6TAR6	0.16	56.52	34.03	D49,E121
GO:0004536	1	A0A351R9X6	0.31	51.52	29.69	Y104,D145,H246
GO:0004550	1	A0A2J7QC69	0.32	60.71	39.67	H162,H316
	2	A0A803K9Z7	0.27	57.14	40.0	H212,H361
	3	D8TIX5	0.4	65.52	40.67	H203,H354
	4	A0A2J7QC53	0.31	60.71	41.33	H231,H385
	5	A0A2J7QC66	0.4	48.15	39.67	H208,H362
GO:0004620	1	P16233	0.21	50.0	36.0	S169,D193,H280
GO:0004725	1	A0A6M8FQ69	0.27	21.43	35.06	C7,R13,D123
GO:0004807	1	A0A840WL33	0.26	81.82	34.57	H93,E163
GO:0004843	1	Q8LAM0	0.31	28.57	38.67	C32,H310
	2	G5E8G2	0.09	66.67	41.67	C60,H307
	3	A0A7D8YLP6	0.06	71.43	50.0	C311,H741
	4	A0A0J8UXP0	0.28	38.1	48.0	C226,H657
	5	O57429	0.21	55.56	42.0	C28,H309
GO:0008080	1	A0A2E8FZC6	0.13	48.0	43.31	E109,Y121
	2	A0A7V7MUE6	0.14	50.0	48.57	E97,Y109
	3	A0A2W1KFP4	0.13	53.85	43.04	E103,Y115
	4	A0A411WMN2	0.24	37.04	46.58	E103,Y115
	5	A0A0U3AA44	0.21	48.0	43.23	E110,Y122
GO:0008106	1	A0A2K6B8V5	0.72	3.7	36.67	E210,C244
	2	O13848	0.19	54.55	41.2	Y54,H109
	3	O13848	0.36	59.09	42.25	Y54,H109
	4	A0A2K5NL52	0.55	3.57	39.67	E210,C244
	5	P30838	0.76	10.0	35.67	E210,C244
GO:0008234	1	P05993	0.15	68.18	51.04	H31,N58
	2	P09648	0.17	74.19	54.59	C25,H165,N185
	3	P83443	0.22	64.71	42.25	C26,H159,N176
	4	P83443	0.17	70.97	46.95	C26,H159,N176
	5	A5YVK8	0.2	76.47	51.63	C14,H146,N162
GO:0015035	1	A0A520C1H0	0.08	66.67	57.32	C7,C10
	2	A0A662FLU1	0.15	87.5	66.67	C30,C33
	3	A0A3D4FEA4	0.21	73.33	58.54	C7,C10
	4	A0A2K5CLF8	0.07	57.14	61.46	C23,C26
	5	A0A7Y2VGP6	0.1	66.67	56.47	C11,C14
GO:0015036	1	A0A182YSM0	0.07	66.67	63.95	C11,C14
	2	A0A1F9KUL7	0.1	73.33	55.56	C32,C35
	3	A0A7V3TX07	0.11	68.75	54.63	C32,C35
	4	A0A550H2S0	0.1	62.5	63.16	C20,C23
	5	A0A3D4FEA4	0.1	80.0	63.41	C7,C10
GO:0016298	1	A0A851Y268	0.23	51.61	36.67	S168,D194,H279
GO:0016407	1	A0A4P7JQ37	0.24	60.0	45.33	E107,Y119
	2	A0A3B9NVM9	0.16	41.67	48.63	E103,Y115
	3	A0A2W4VE46	0.23	61.54	48.67	E105,Y117
	4	A0A0P6VE99	0.76	50.0	45.62	E111,Y123
	5	A0A654L334	0.26	46.15	41.72	E99,Y111
GO:0016408	1	Q7A1P9	0.15	61.9	43.33	C86,H338
GO:0016410	1	D4XNE3	0.2	76.0	44.44	E99,Y111
	2	A0A6N6RS47	0.72	36.0	44.59	E104,Y116
	3	A0A2L1WHT7	0.25	52.0	48.67	E105,Y116
	4	A0A6N1N5Z4	0.19	64.0	42.76	E99,Y111
	5	A0A7C5L4R9	0.65	33.33	41.96	E97,Y109

Term	Sample	AFDB / UniProt ID	Active site RMSD	5 Å ID	Seq. ID	Active site residues
GO:0016419	1	A0A3B0J3W0	0.18	53.85	37.0	S92,H201
	2	A0A077PZH2	0.17	46.43	41.67	S92,H201
	3	A0A0K2ART5	0.24	61.54	32.67	S89,H193
	4	A0A416WG28	0.27	53.85	30.67	S87,H198
	5	A0A3D3W9N5	0.28	46.15	35.0	S90,H195
GO:0016420	1	A0A2D4TSP9	0.08	57.14	36.0	S90,H198
	2	A0A1C6NL35	0.11	56.0	36.67	S88,H193
	3	A0A536FEV0	0.27	48.15	43.0	S114,H221
	4	H2IQE4	0.3	52.0	23.33	S86,H195
	5	A0A101C5L5	0.22	46.15	33.67	S87,H195
GO:0016620	1	A0A7C7GGH8	0.14	66.67	31.0	E161,C195
	2	A0A3D0RY98	0.12	58.82	40.67	E232,C266
	3	A0A511J2Y8	0.16	66.67	46.33	E253,C287
	4	A0A1M5N6Y7	0.22	61.54	48.33	E233,C267
	5	A0A1R3FFM7	0.21	70.37	41.33	E217,C251
GO:0016667	1	A0A522QSK5	0.27	10.53	51.82	C32,C35
	2	A0A352HRW1	0.04	62.5	59.3	C7,C10
	3	A0A3D4FEA4	0.08	47.06	54.88	C7,C10
	4	A0A352PK77	0.1	80.0	51.92	C30,C33
	5	A0A3C0KDU2	0.04	50.0	70.15	C34,C37
GO:0016855	1	A0A256BFD5	0.28	19.05	30.43	C78,C187
GO:0016864	1	Q0E0I1	0.09	90.0	39.67	C75,C78
GO:0016884	1	E0NNP0	0.21	64.52	44.33	K69,S144,S168
GO:0030060	1	K0J107	0.28	55.0	40.33	D173,H200
	2	K0J107	0.23	76.19	40.33	D173,H200
	3	K0J107	0.36	52.38	40.0	D173,H200
	4	K0J107	0.32	63.64	39.0	D173,H200
GO:0032296	1	A0A149VUG9	0.21	50.0	37.83	D47,E119
	2	Q2NB81	0.18	50.0	39.01	D48,E119
GO:0033818	1	A0A535CXZ2	0.24	65.62	44.0	C129,H260,N290
	2	A0A0J9FDV5	0.25	54.55	32.33	C116,H256,N286
	3	A0A2V5ZBS8	0.59	33.33	35.67	C127,H267,N297
	4	A0A2V3W4S1	0.53	37.5	32.0	C112,H237,N267
	5	A0A6I3ZG68	0.61	35.29	40.33	C122,H258,N289
GO:0047661	1	A0A252DYH1	0.23	25.0	26.62	C91,C200
	2	A0A0R2B670	0.36	56.0	40.21	C73,C184
	3	A0A5M8R285	0.26	52.0	25.28	C75,C188
	4	R7IW21	0.58	31.82	25.9	C79,C190
GO:0051920	1	A0A3P1CPV9	0.12	26.67	33.67	C158,C161
	2	A0A243RTW8	0.15	53.33	41.57	C131,C134
GO:0052689	1	A0A4Y8L3A9	0.32	32.26	28.0	S93,D192,H222
	2	A0A2E9H3J6	0.25	41.94	32.55	S81,D206,H234
	3	A0A4R0ZJD2	0.22	35.71	29.48	S98,D194,H223
	4	A0A7X1TML9	0.35	44.83	30.33	S186,D277,H306
	5	A0A523I713	0.32	44.83	27.0	S169,D255,H285
GO:0052745	1	Q3ZCK3	0.13	47.62	34.0	D51,T122
	2	Q9Z0S1	0.64	33.33	32.0	D51,T122
GO:0070001	1	A0A1Y1ZC50	0.09	60.87	33.33	D17,D198
	2	A0A818CU57	0.12	69.57	48.0	D304,D485
	3	A0A3B5Y713	0.49	59.09	35.33	D126,D349
	4	F9XJD5	0.2	56.52	32.0	D91,D273
	5	A0A667INK2	0.12	60.87	35.67	D94,D281

Term	Sample	AFDB / UniProt ID	Active site RMSD	5 Å ID	Seq. ID	Active site residues
GO:0070008	1	Q8L9Y0	0.22	67.86	48.67	S185,D395,H447
	2	Q9CAU2	0.49	46.67	32.33	S183,D363,H416
	3	Q869Q8	0.34	58.62	38.33	S233,D414,H474
GO:0101005	1	A6NNY8	0.14	71.43	42.33	C87,H380
	2	Q9LEW0	0.14	71.43	45.33	C186,H491
	3	P62068	0.15	65.0	42.67	C44,H313
	4	Q52KZ6	0.13	66.67	43.33	C48,H317
	5	Q9FPS3	0.17	61.11	45.67	C206,H510